UNITED NATIONS EDUCATIONAL, SCIENTIFIC AND CULTURAL ORGANIZATION
INTERNATIONAL ATOMIC ENERGY AGENCY
INTERNATIONAL CENTRE FOR THEORETICAL PHYSICS
I.C.T.P., P.O. BOX 586, 34100 TRIESTE, ITALY, CABLE: CENTRATOM TRIESTE

SMR.998c - 9

Research Workshop on Condensed Matter Physics
30 June - 22 August 1997

MINIWORKSHOP ON
PATTERN FORMATION AND SPATIO-TEMPORAL CHAOS
28 JULY - 8 AUGUST 1997

"Spirals and scrolls in the Belousov-Zhabotinsky reaction"

"Forcing and control of excitation waves"

"How social amoebae find each other"

"Spreading depression waves in neuronal tissue"

Stefan C. MÜLLER
Otto-von-Guericke Universitat
Inst. fur Exp. Physik
Postfach 4120
D39016 Magdeburg
GERMANY

These are preliminary lecture notes, intended only for distribution to participants.

Experiments on Excitation Waves

S.C. Müller

Max-Planck-Institut für molekulare Physiologie, Rheinlanddamm 201, D-44129 Dortmund, and
Otto-von-Guericke-Universität Magdeburg, Institut für Experimentelle Physik, Universitätsplatz,
D-39106 Magdeburg, Germany

Abstract. Recent trends in the experimentation on chemical and biochemical excitation waves are presented. In the Belousov-Zhabotinsky reaction, which is the most suitable chemical laboratory system for the study of wave propagation in excitable medium, the efficient control of wave dynamics by electrical fields and by light illumination is illustrated. In particular, the effects of a feedback control are shown. Further new experiments in this system are concerned with three-dimensional topologies and boundary effects. Important biological applications are found in the aggregation of slime mould amoebae, in proton waves during oscillatory glycolysis, and in waves of spreading depression in neuronal tissue as studied by experiments in chicken retina. Numerical simulations with appropriate reaction-diffusion models complement a large number of these experimental findings.

1. Excitation waves

Traveling waves of excitation are abundant in biology, for instance, in slime mould aggregation (Siegert and Weijer, 1992), frog oocytes (Lechleiter et al., 1991), heart muscle (Davidenko et al., 1992), or chicken retina (Gorelova and Bures, 1983). They are also plentiful in physical and physico-chemical systems and recent overviews are available (Kapral and Showalter, 1995; Müller et al., 1994). The interest in exploring their properties has continuously increased during the last decades, because these waves exhibit, due to their nonlinear nature, an amazing richness in dynamic shapes and patterns.

This article is not intended to review all the exciting aspects of current research on such traveling waves. It will just highlight several recent research directions that are followed in the author's own laboratory. These activities may give, to some extent, an impression for a more general tendency that research on such selforganized structures will take in the near future.

The best known laboratory system for the study of excitation waves is the Belousov-Zhabotinsky (BZ) reaction which is the bromination of malonic acid in acid medium. Much experimental and numerical work has been devoted to study wave phenomena in thin layaer of excitable reaction mixtures, either circular concentric waves (target patterns) triggered externally by a local disturbance (a silver wire, for instance) or rotating spiral waves that

develop from broken wave ends. Figure 1a shows a pair of counter-rotating spirals as observed in a variant of the BZ reaction in which a cerium compound serves as the catalyst and indicator. In this case the wave crests, that is the excited areas of highest catalyst oxidation, appear dark in transmitted light, because at the chosen observation wavelength in the UV range (340 nm) only the oxidized form of the catalyst absorbs light substantially, while the reduced form does not. This is in contrast to the usual picture of bright wave crests on a dark background, as we know it from the much more popular ferroin-catalyzed reaction, in which the oxidized form is the absorbing species (in that case the observation wavelength lies in the visible range at 490 nm).

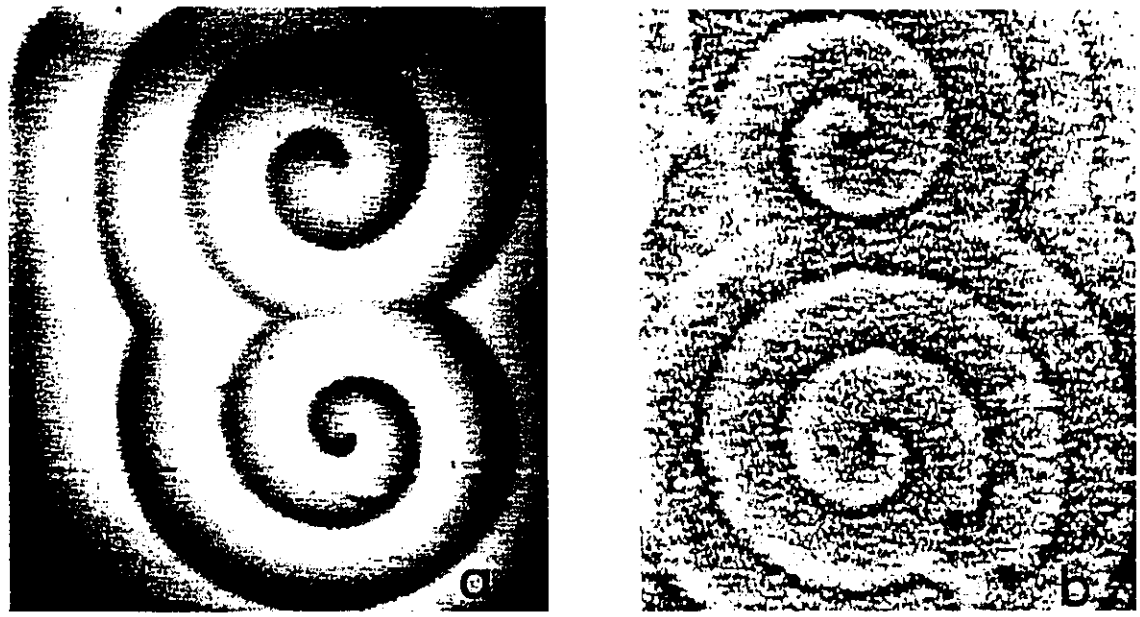

Fig. 1. (a) Pair of counterrotating spiral waves in the cerium-catalyzed BZ-reaction, observed in transmitted light (λ=340 nm). Image area: 1x1 cm^2 (b) Darkfield photograph of an early stage in the aggegation of slime mould amoebae. Dark and bright lines indicate the spiral-shaped, chemotactic motion field directed towards the spiral center. Image area: 1.9x1.9 cm^2 (from Foerster et al., 1990).

The second picture in Fig. 1 shows an example for excitation waves found in a biological system that obviously has structural features quite analogous to the chemical waves in image (a). It is a dark-field photograph of aggregation waves in colonies of slime mould amoebae (*Dictyostelium discoideum*). The pattern is due to differences in light scattering behavior of moving and resting amoebae cells. With each turn of the spirals a chemotactic response to the spiral-shaped distribution of the signal transmitter molecule cAMP results in a gradual displacement of the cell population towards the spiral centers. With persisting rotation of this concentration distribution a signalling mechanism is set up that gathers many single cells in the central spiral region where they grow together to form a multicellular slug. This is an important step in the lifecycle of this population.

Particular interest lies in the study of the tip dynamics of such spirals, because the trajectory of the tip can follow quite different traces depending on the preparation of the system in terms of its excitability and threshold of excitation (Jahnke and Winfree, 1991). The most commonly known regime is that of rigid rotation of the tip, as observed in certain standard preparations of the BZ reaction (Fig. 2a). Also the spirals in the BZ reaction and in the slime mould shown in Fig. 1 follow such a rigid regime. It turns out, however, that the more frequent case is a hypocycloidal (or "meandering") tip motion in which at least 2 frequencies - a small and a much larger one - determine the resulting compound trajectory (Fig. 2b). These floral trajectories may have a quite different number of lobes under different initial conditions. In extreme cases the cycloidal motion turns into a „loopy line" along which the spiral drifts towards the boundary of the dish (Fig. 2c). When the excitability of the system is decreased, the regularity of the pattern dynamics may be replaced by a rather irregular motion (see the example in Fig. 2d). These changing aspects of the intrinsic spiral dynamics have been systematically studied in the BZ reaction and corresponding numerical simulations exist on the basis of mathematical models for excitable reaction-diffusion systems (for an overview see corresponding chapters in the volumes by Kapral and Showalter, 1995; Müller et al., 1994).

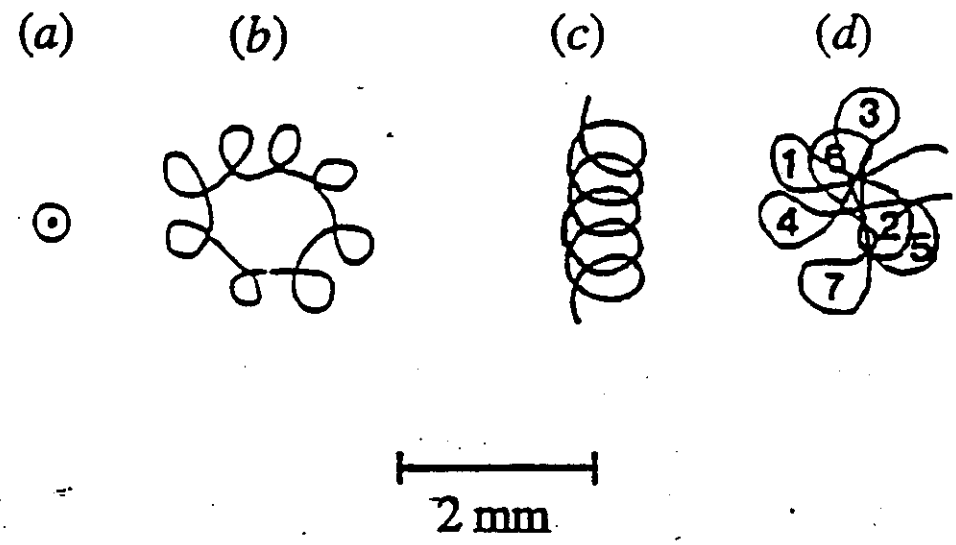

Fig. 2. Typical trajectories of spiral tip motion measured in the BZ-system. (a) rigid rotation, (b) hypocycloidal trajectory (meander), (c) loopy line, (d) irregular motion (from Nagy-Ungvarai et al., 1993).

2. New trends in the investigation of chemical excitation waves

Nowadays there is a large interest in subjecting the chemical waves, in particular spiral-shaped ones, to external forces in order to find ways how to influence and control their intrinsic dynamics. There are at least two methods that provide efficient tools for such an external influence: application of an electric field acting on the motion of charged species in

the BZ reaction, and illumination of a photo-sensitive variant of this reaction that reduces its excitability with the applied light intensity.

2. 1. Control by electric field

The effect of an electric field on spatial patterns in the BZ reaction was first studied by Feeney et al. (1981). Later Sevcikova et al. (1983, 1992) found that in a small glass capillary, an approximately one-dimensional system, applying an electric field can cause a chemical wave propagating towards the anode to accelerate. Changing the polarity may stop or split the wave, depending on the strength of the field. Accordingly, spiral waves are subjected to a drift in space accompanied by spiral deformation and changes in wavelength due to the Doppler shift. With the appropriate field polarity, the drift can be used to induce a mutual approach of a spiral pair when starting such as shown in Fig. 1a (for this purpose the anode has to be located at the right hand side of the spiral pair, cf. Fig. 3). As demonstrated by Schütze et al. (1992) the spiral approach leads at sufficiently high field strength to mutual annihilation of the spiral pair or to a rather complex interaction of their cores, which tend to avoid each other and thus reveal a high degree of stability.

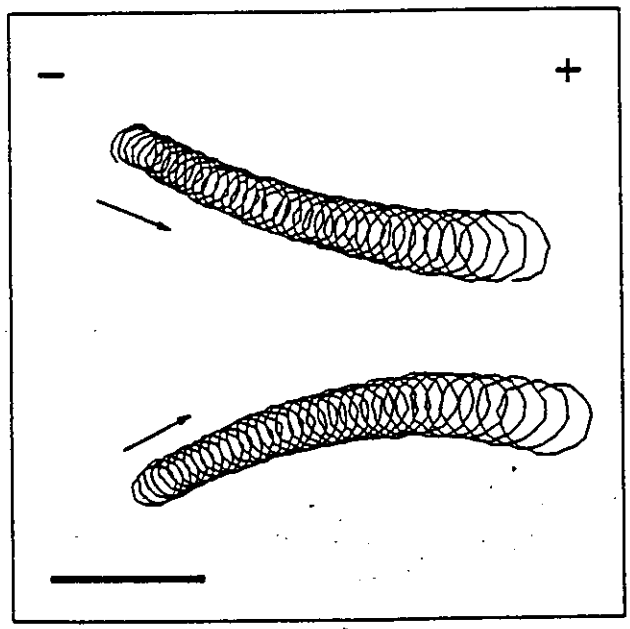

Fig. 3. Tip trajectories of a spiral pair such as shown in Fig. 1a moving towards each other under the influence of an externally applied electric field. At the selected field strength the drift of the rotating spiral tips becomes asymptotically parallel. Scale bar: 1mm (from Schmidt, 1995).

In extension of this work it was shown recently by Schmidt (1995) that with moderate field strength and when starting from a highly symmetric pair of counter-rotating spirals (with respect to their phase of rotation) the interaction results in a parallel drift (see asymptotic behavior in Fig. 3). During the drift a distance which depends on the applied field strength is

maintained between the spiral cores. This finding corroborates the stability of the spirals: only when a certain threshold of the field strength is exceeded, the spirals approach leads finally to mutual annihilation.

2. 2. Control by light

Another efficient tool for external control of spiral wave parameters is found in the light-sensitive, ruthenium-catalyzed preparation of the BZ reaction. If the ruthenium complex is photochemically excited, it catalyzes the production of the inhibitor species of the reaction, the bromide ion (Kuhnert, 1986). This way an externally applied illumination reduces or completely suppresses the excitability of the medium. Although the mechanistic details of the bromide production are still under discussion (see Mori et al., 1993), a large number of possibilities have already been explored to make use of this effect, for instance, by local application of a high-intensity laser beam (Steinbock and Müller, 1993). This way artficial spiral cores can be placed at a particular site to which the spiral tip remains anchored. The laser beam creates a disk, the radius of which determines the spiral wavelength.

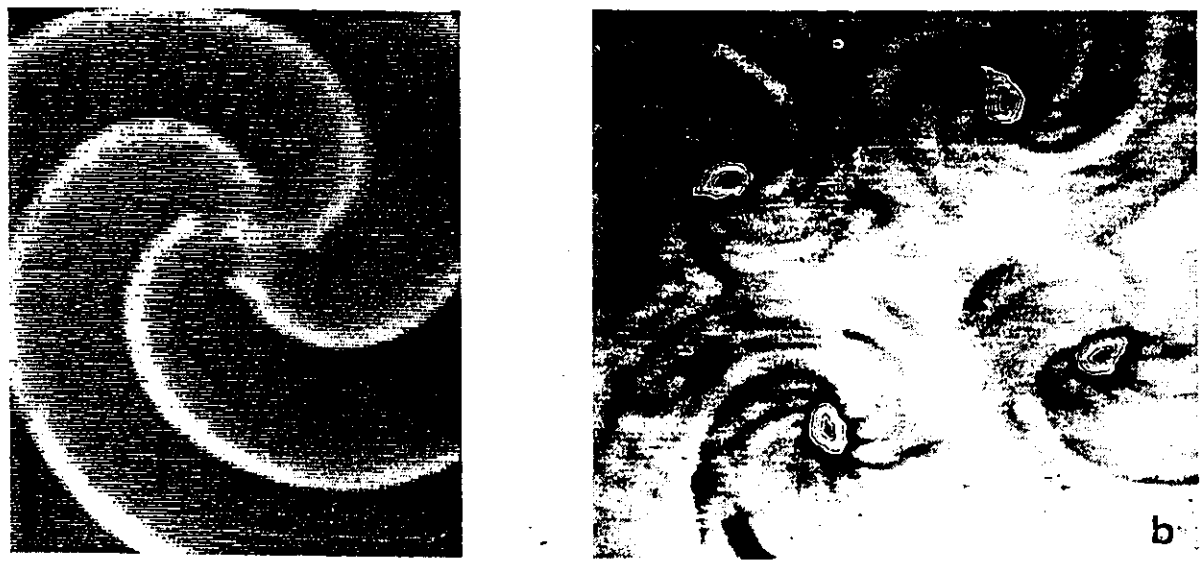

Fig. 4. (a) Collision structure in the central region of a four-armed spiral in the ruthenium-catalyzed Belousov-Zhabotinsky reaction. (b) Digital overlay of 36 consecutive snapshots of the four-armed spiral. The shape of the four spiral cores is outlined by a dense sequence of contour lines. Image area: 20 mm (compare Steinbock and Müller, 1993).

Such a disk can also be used to construct multi-armed spirals with spiral tips rotating at equal distances around the disk boundary. After switching off the laser beam these multiple tips move synchronously into the area of the previously unexcitable area, where they collide with each other as shown in Fig. 4a. An overlay technique applied to a temporal sequence of digital images of this structure covering several rotation periods reveals that four stationary

and well separated cores exist in this experiment (Fig. 4b). The interesting observation was made, that spiral arms are not constantly attached to one of the individual cores: During one period, each arm is passed round to the neighboring core in the sense of individual spiral rotation („round dance" of the waves).

If illumination is applied globally to the photosensitive reaction layer, one can control the dynamics of spirals in the entire system by periodic modulation of (moderate) light intensity (Steinbock et al., 1993; Braune and Engel, 1993). The modulation of excitability forces meandering spiral tips to phase-locked motion, a spectrum of open and closed hypocycloidal trajectories, and complex multifrequency patterns. These experimental results are reproduced by numerical simulations with a two-variable Oregonator model, which was extended by a term describing the light-induced bromide production. They show the existence of entrainment bands in the plane of modulation period and amplitude.

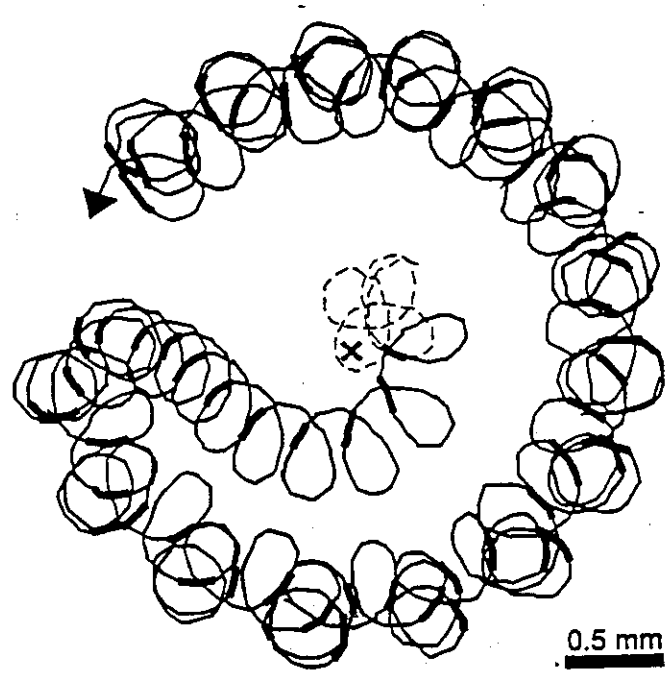

Fig. 5. Feedback-controlled, pulse-like illumination leads to spiral tip motion that describes asymptotically a regime called resonance attractor. Thick segments correspond to time intervals of light pulses applied after a front has moved through point (x). Dashed line indicates the initial unperturbed trajectory (from Grill et al., 1995).

While so far the wave dynamics was influenced by an independent external source, the question arises, whether some kind of feed-back loop could establish a coupling between the intrinsic pattern properties and the external influence on them. We realized a feed-back control in the following way: The external signal consists of a sequence of short light pulses, lasting several seconds. Each single light pulse deforms the trajectory of the spiral tip in a

characteristic way. An arbitrary measuring point is chosen at some distance from the tip which, in these experiments, described a four-lobed meandering trajectory (dashed curve in Fig. 5). Every time when a wave front emanating from the spiral center reaches the measuring point (at location „x" in Fig. 5) a short light stimulus was triggered immediately or with a certain time delay after the wave front passage. Thus, when the feedback mechanism is switched on, the spiral is forced by a sequence of short impulses. The influence of each stimulus is overlaid with the effect of the previous ones.

Quite surprisingly, this feedback procedure has lead to the observation of two new regimes, which we call „entrainment" and „resonance" attractors (Grill et al., 1995): If the measuring (and control) point is chosen rather close to the central region of the unperturbed tip trajectory, the feedback results in a strictly synchonized relationship between the tip motion and the sequence of external stimuli. The spiral tip approaches an asymptotic trajectory with a symmetry center that coincides with the control point. It loops around this center and each stimulus is applied at the same phase of the individual loops (entrainment). If on the other hand the control point is chosen far from the unperturbed trajectory, one observes the evolution shown in Fig. 5. The spiral tip approaches again a stable trajectory which, in this case, looks like a drift of the original four-lobed hypocycloid along a large circle. Its center coincides again with the measuring point. Differences to the former regime are: the sense of core rotation around the measuring point is opposite, the sequence of light stimuli is not precisely periodic, and the stimuli are applied at different phases of the lobes. Due to similarities with the so-called resonace drift observed in previous work (Zykov et al., 1994), this regime is called resonance attractor.

Both attractors are stable with respect to small shifts of the control point. A separatrix between them has not yet been determined. Introduction of a delay time leads to changes in the average attractor radius. All these features are also found in simulations performed with the Oregonator reaction-diffusion model (Grill et al., 1995). The nice feature of this feedback mechanism is its potential to control efficiently the path of a spiral wave by using only moderate global perturbations. The choice of a particular control point and a delay time suffice to predetermine the future evolution of a rotating excitation wave.

2.3. Boundary effects

Usually the radius of a spiral wave core is very small with respect to the size of the Petri dish and the boundary conditions do not influence the tip motion in common chemical experiments. Recently, some work was devoted to elucidate the possible role of a non-flux boundary (Müller et al., 1995; M. Gomez-Gesteira et al., 1996). We used a special technique to study the role of the boundary in excitable BZ gel medium. We cut a small disk (diameter 2 - 3 mm) of a gel by a cylinder with a thin wall, selecting an area of the medium surrounding

the tip of a spiral wave created beforehand in the dish. Then the further circulation of the vortex occurred in this small disk of the gel. (see Fig. 6).

Due to the small size of the system the following evolution of the spiral is subjected, in fact, to a pronounced influence of the boundary and depends on the initial location of the wave inside the disk. As a rule, the boundary attracts the spiral core. Sometimes it leads to a fast motion towards the boundary and the death of the spiral. But rather often spirals start to move along the system boundary. In this case the spiral tip describes a quited complicated trajectory. In principle, the shape of the trajectory is very similar to an epicycloid. One can distinguish the motion around a circular core and the drift of the core along the boundary. During the drift the characteristic distance from the center of the core to the boundary is about 0.3 mm. This drift occurs with a velocity of about 0.15 mm/min.

A non-flux boundary for which Neumann boundary conditions hold can be regarded as a virtual mirror and the medium can be extended by its "mirror reflection". In this case one can assume that a single spiral close to the border will interact with the border as if it were interacting with the "mirror reflection" of itself. In this sense the drift behavior close to the border becomes comparable with the parallel drift of a vortex pair in electric field as shown in Fig. 3.

Fig. 6. A spiral rotating in a small gel disk of excitable Belousov-Zhabotinsky medium (diameter 2mm). Its tip trajectory is frequently found to drift along the boundary of this domain at a certain distance.

2.4. Three-dimensional topologies

Spiral waves, as commonly observed in thin layers of the BZ reaction (cf. Fig. 1a), may be regarded as suitably oriented cross-sections of so-called scroll waves in a three-dimensional medium (see review by Tyson and Strogatz 1991). As a particularly interesting example we

show in Fig. 7(a-f) the spectrophotometric projection of a „scroll ring" at six different stages during one cycle of spiral rotation. The reactive BZ medium is contained in a rectangular cell of both 10 mm width and thickness. The circular edge of the scroll ring rotates periodically around a 3-D curve called filament, which in this case forms a closed ring (see closed ellipse in the projections of Fig. 7b-d). However, the propagation of the wave edge is slightly faster during phase (b,c) as compared with (e,f) due to the different sign of curvature along the filament. Thus the filament gradually contracts and finally, once a critical filament diameter is reached, opposed parts of the wave edges collide during the phase corresponding to Fig. 7 (b-c), before proceeding through the opening of the filament as in (d).

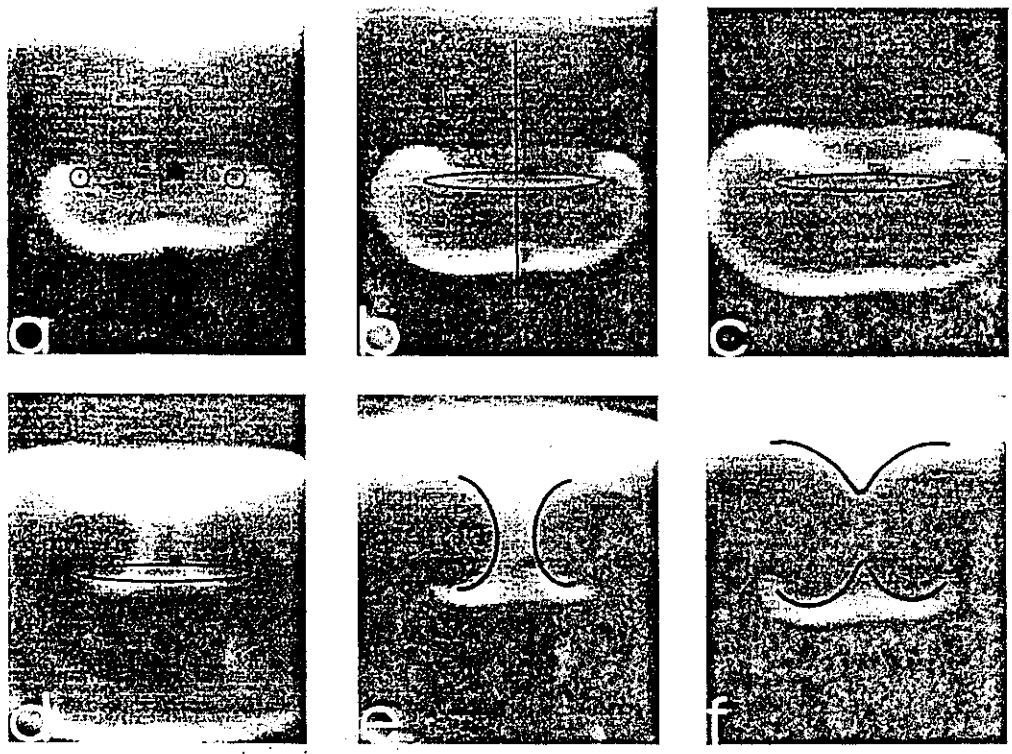

Fig. 7. Scroll ring in the ferroin-catalyzed BZ reaction. Sample thickness and width 10 mm, respectively. As seen in projection, the wave resembles a pair of spiral waves undergoing rigid rotation (circles in a). At any phase the actual 3-D wave structure has rotational symmetry (axis in b). The leading wave edge is scrolling around a circular filament (slim ellipse in b-d). After the wave edge has passed through the filament, certain segments of the wave front approach the symmetry axis (enhanced contours in e). Due to collision the leading part of the wave segregates (in f) to start a new cycle (period about 3 minutes).

A quantitative study of scroll waves with less symmetry than the scroll ring is not possible by only using projections under a fixed angle of view. Recently an optical tomographic technique has been established that provides 3D reconstructions of chemical waves of arbitrary shape in the BZ reaction (Stock and Müller, 1996). Thus, further experiments with more complicated filament dynamics will be facilitated. But the preparation

of suitable initial conditions for more complex 3D waves is still an unsolved experimental problem. These structures are, for example, characterized by a knotted filament or two circular rings linked to one another and were already investigated in numerical simulations (see Winfree 1995 and references therein). In contrast to experimental observations of scroll rings, these do not finally undergo self-annihilation, but stabilize at a certain size and shape. The balancing repulsion against curvature-induced filament contraction is putatively attributed to an interaction with a twist (i. e. a phase shift) of the wave edge along the filament, but this effect remains to be investigated experimentally.

3. Excitation waves in biological systems

3.1. Glycolysis in extract from yeast cells

Sugar degradation via glycolysis is a central metabolic pathway in all eucaryotic cells and has been the subject of intense biochemical as well as genetic work (reviewed by Hess and Boiteux, 1971; Fothergill-Gilmore et al., 1992). Under substrate-limited conditions the glycolytic flow proceeds in an oscillatory manner, resulting from feed-back regulation of the allosterical enzyme phosphofructokinase (Hess et al., 1968). Since glycolysis is characterized by a nonequilibrium state and nonlinear rection kinetics, self-organization is likely to occur and has been predicted by earlier theoretical studies (Goldbeter, 1973). But it was not until recently that findings from our laboratory (Mair and Müller, 1996) and a Japanese group (Shinjyo et al., 1995) confirmed this prediction. We found that traveling NADH and proton waves develop spontaneously in a yeast extract that exhibits oscillatory sugar degration. Wave annihilation (Fig. 8a) as well as spontaneous break-up of circular wave fronts and subsequent formation of rotating spirals (Fig. 8b) could be observed. A crucial role for the control of pattern dynamics and wave initiation could be attributed to the autocatalytic reaction of glycolysis catalyzed by the phosphofructokinase. More complicated patterns were reported for a yeast extract fixed in gel (Shinjyo et al., 1995) and some actual attempts are being done to produce stationary Turing-type patterns in this biochemical model system by using an open gel reactor of the type introduced by Skinner and Swinney (1991).

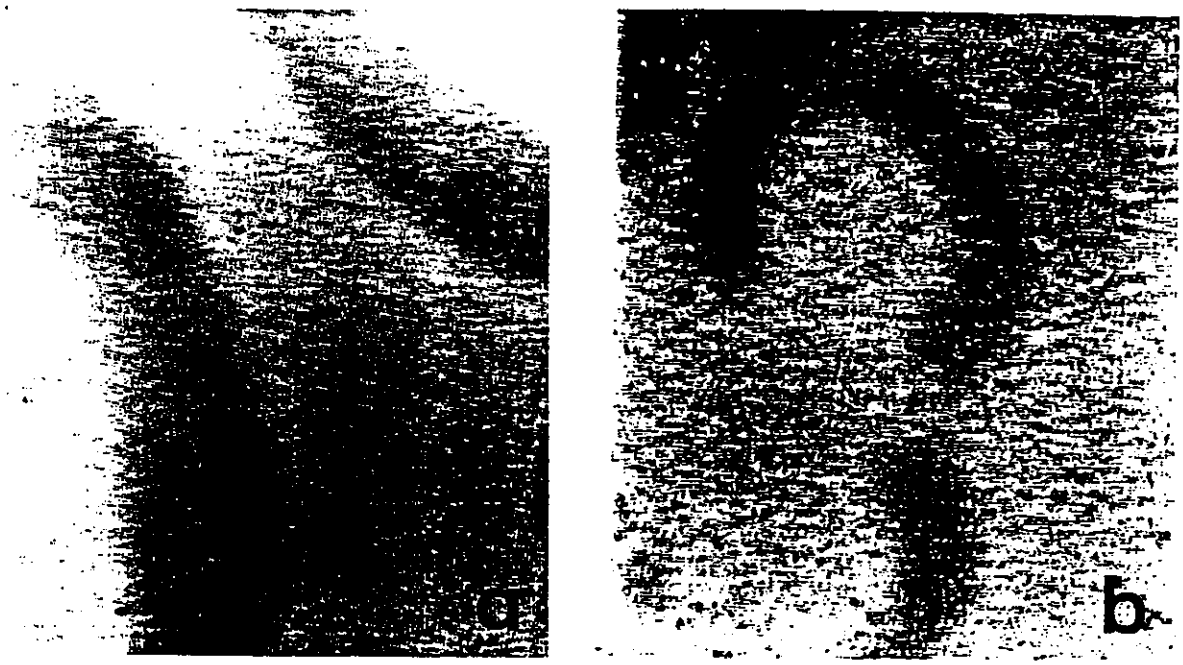

Fig. 8. (a) Section of circular waves of NADH propagating towards each other in a cell-free extract from yeast, observed in light transmission (λ=340 nm). (b) Broken ends in the same system tend to curl up to form spirals.

3.2. Spreading depression waves

Spreading depression (SD) is a dynamic wave phenomenon occurring in most gray matter of the central nervous system (CNS) (Bures et al., 1974; Leao, 1944). SD shares significant features with ischaemi and anoxia (Hansen, 1985) and is further linked to migraine, epilepsy and post-traumatic syndroms (Gordon, 1989). The retina, especially the isolated chicken retina, is an excellent constituent of the CNS to observe the dynamic behavior of the spreading depression (SD) wave fronts, because it changes its optical properties during a SD attack (Gorelova and Bures, 1983). The waves become visible as milky fronts on a black background. It is still controversial, which are the basic mechanistic steps of SD, but certainly SD belongs to the self-organization phenomena occurring in neuronal tissue.

We analyzed the dynamics of spiral-shaped wave fronts using digital video imaging techinques (Dahlem and Müller, 1996): The inner end of the wave front, the spiral tip, breaks away repeatedly. This separation process is associated with a Z-shaped trajectory (extension, ~1.2 mm) that is described by the tip over one spiral revolution (period, 2.45±0.1 min). Fig. 9 illustrates this unusual tip motion by an digitized overlay of several snapshots taken during one spiral period. The Z-shaped trajectory does not remain fixed, but performs a complex motion across the retina with each period. The self-induced splitting process and the formation of the complex trajectory are very perculiar features of intrinsic spiral tip dynamics in the chicken retina and, to our knowledge, have not been observed in any other excitable medium (compare Fig. 2).

Fig. 9. Image of the intrinsic optical signal of spreading depression in the retina. Overlay of 13 subsequent spiral waves (time interval between subsequent images, 12.6 s). The core of the spiral center exhibits the Z-shaped path of the spiral tip.

4. Numerical simulations

Models of excitable kinetics coupled with diffusion have been very successful to explain many of the generic features of pattern formation and dynamics found in experimental work. Especially, the Oregonator based reaction-diffusion model by Keener and Tyson (1986) and appropriate variations or extensions of this model prove to be able to reproduce many of the spatio-temporal characteristics of the BZ reaction, both with respect to its intrinsic dynamics (cf. Section 1) and the response to external perturbation and control described in Section 2. However, this model description still fails to provide quantitative recipes or guidelines for the experimentator, and a direct comparison between theoretical and experimental system parameters can not yet been made in general.

We present here briefly the results of a numerical investigation for which experimental verification is still mostly missing. The evolution of spiral waves on a circular domain and on a spherical surface was studied by numerical integration of a reaction-diffusion system. For this purpose an original computational scheme was elaborated for two-dimensional domains with rotational symmetry (Davydov and Zykov, 1993; Müller et al., 1995). This explicit scheme uses a polar coordinate system with a nonuniform computational grid. It results in a quasi-uniform distribution of computational nodes in the Cartesian coordinate system. By this procedure difficulties in using the polar coordinate system are effectively circumvented.

One should assume a priori that waves processes on a circular and spherical domain turn out to have quite different characteristic features. Our computations demonstrate, however, that there is a close similarity between the dynamics of spiral waves in these two different geometries (Zykov et al., 1996). Two different asymptotic regimes are observed for both domains. The first regime is a rigid rotation of an excitation wave around the symmetry axis of the domain. The second one is a compound rotation including a drift of the rotation center of the spiral wave either along the boundary of the disk or along the equator of the sphere. In this case the shape of the wave and its rotation velocity are periodically changing in time.

An example of stationary rotation of a excitation wave on a sphere is shown in Fig. 10a. This wave has two open ends. The trajectory of each open end circumscribes a spiral wave core with a center located at the corresponding pole. The form of the wave and the angular velocity of its rotation depend on the radius of the sphere. A quite different regime is observed, when the open ends are initially placed near the equator. In this case the propagating wave never achieves a stationary regime. One observes, instead, periodic pulsations in the shape and the rotation velocity of the spirals. The trajectory of the open ends look like a cycloid placed on the sphere (Fig. 10b). These open ends rotate around some cores, but the cores do not include the poles, in contrast to the previous case of stationary rotation. Moreover, the cores move with a constant speed along a specific latitude. This speed determines a second period in the considered problem, in addition to the rotation around the cores.

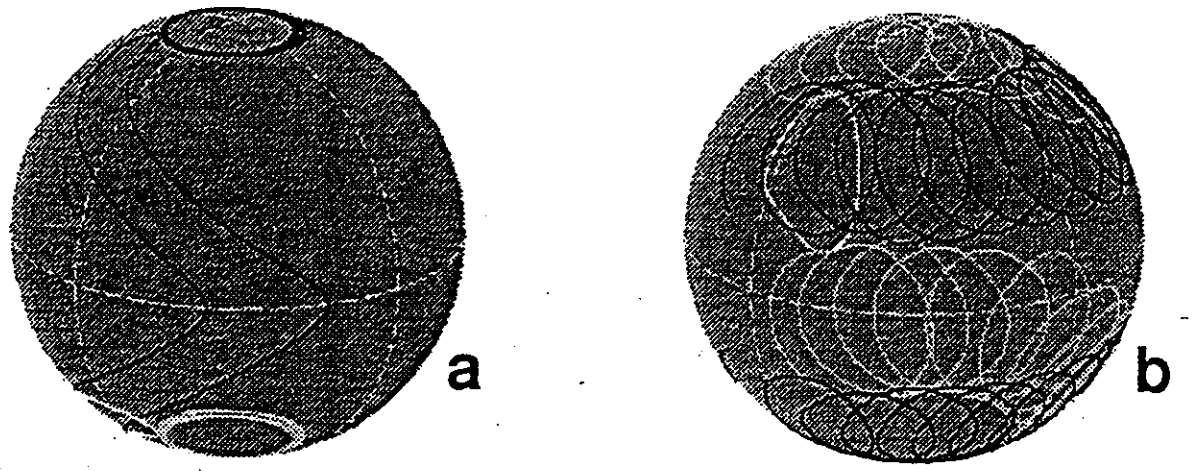

Fig. 10. Numerical simulation of spiral waves on a sphere. (a) Stationary rotation around the symmetry axis with cores located at north and south pole; (b) cycloidal (two-periodic) regime with cores moving along some latitude. The black (white) curves present the wave contour and tip trajectory on the visible (hidden) part of the sphere.

One can note a close analogy between such a two-periodic regime on a sphere and on a disk as described in Section 2.3. (see Fig. 6). Indeed, the wave patterns observed in our computations on a sphere are symmetric with respect to the equator plane. Hence, the equator

can be considered as a non-flux boundary imposing a restriction on each of the hemispheres. Topologically each of the hemispheres is very similar to a disk restricted by a circular non-flux boundary.

5. Outlook

Recent developments in the field of oscillating and excitable reactions allow to study much more complex regimes and wave patterns in spatially extended systems than previously expected. It has become possible now for the experimentalist to be not only passive observer of the "life" of a spiral, but to govern the growth, evolution, and decay of spiral populations by choosing sets of external parameters and the proper geometry of the medium. Gel techniques, electric fields and the use of photosensitive variants of the BZ reaction have become most important tools for applying well-controlled global or local perturbations to the system and precisely change the parameters in the desired direction. These advantages underline the role of the BZ reaction as an extremely valuable instrument for the modelling of self-organization processes as they frequently occur in biological excitable systems.

Starting from some of the actual work outlined in this contribution, future trends may be forseeable, for instance, the growing importance of control features and their application to collective self-organized cell motion in early stages of morphogenesis, to cardiac arrhythmias (Winfree, 1987), or to the spatio-temporal dynamics of cortical phenomena.

References

Braune, M. and Engel, H. (1993): Compound rotation of spiral waves in a light-sensitive Belousov-Zhabotinsky medium. Chem. Phys. Lett. **211**, 534

Bures, J., Burešová, O., and Krivánek, J. (1974): The mechanism and applications of Leão's spreading depression of electroencephalograpic activity (Academic Press, NewYork)

Dahlem, M.A. and Müller, S.C. (1996): Self-induced splitting of spiral-shaped spreading depression waves in chicken retina, submitted to Experimental Brain Research

Davidenko, J.M., Pertsov, A.V., Salomonsz, R., Baxter, W., and Jalife, J. (1992): Stationary and drifting spiral waves of excitation in isolated cardiac muscle. Nature **355**, 349

Davydov, V.A. and Zykov, V.S. (1993): Spiral waves in a round excitable medium. JETP **76**, 414

Feeney, R., Schmidt, S., and Ortoleva, P. (1981): Experiments on electrical field - chemical wave interactions: Annihilation and the crescent wave. Physica **2D**, 536

Foerster, P., Müller, S.C., and Hess, B. (1990): Curvature and spiral geometry in aggregation patterns of Dictyostelium discoideum. Development **109**, 11

Fothergill-Gilmore, L.A. and Michels, P.A.M. (1992): Evolution of glycolysis. Prog. Biophys. molec. Biol. **59**, 105

Goldbeter, A. (1973): Patterns of spatiotemporal organization in an allosteric enzyme model. Proc. Natl. Acad. Sci. USA **70**, 3255

Gordon, N. (1989): Migraine, epilepsy, post-traumatic syndromes, and spreading depression. Dev. Med. Child. Neurol. **31**, 682

Gómez-Gesteira M., Muñuzuri A. P., Pérez-Muñuzuri V., Pérez-Villar V. (1996): Boundary-imposed spiral drift. Phys. Rev. **E 53**, 5480

Gorelova, N. A. and Bureš, J. (1983): Spiral waves of spreading depression in the chicken retina, J. Neurophysiol. **14**, 353

Grill, S., Zykov, V.S., and Müller, S.C. (1995): Feedback-controlled dynamics of meandering spiral waves. Phys. Rev. Lett. **75**, 3368

Hansen, A. J.(1985): Effect of anoxia on ion distribution in the brain. Physiol. Rev. **65**, 101

Hess, B. and Boiteux, A. (1971): Oscillatory phenomena in biochemistry. Ann. Rev. Biochem. **40**, 237

Hess, B., Boiteux, A., and Krüger, J. (1968): Cooperation of glycolytic enzymes. Adv. Enzym. Regul. **7**, 149

Jahnke, W. and Winfree, A.T. (1991): A survey of spiral-wave behaviors in the Oregonator model. Int. J. Bifurcation and Chaos **1**, 445

Kapral, R. and Showalter, K. (eds.): Chemical Waves and Patterns (Kluwer, Dordrecht, 1995)

Keener, J. P.and Tyson, J. J. (1986): Spiral waves in the Belousov-Zhabotinskii reaction. Physica D **21**, 307

Kuhnert, L. (1986): A new optical photochemical memory device in a light-sensitive chemical active medium. Nature **319**, 393

Leão, A.A.P. (1944): Spreading depression of activity in cerebral cortex. J. Neurophysiol. **7**, 359

Lechleiter, J., Girard, S., Peralta, E., and Clapham, D. (1991): Spiral calcium wave propagation and annihilation in Xenopus laevis oocytes. Science **252**, 123

Mair, T. and Müller, S.C. (1996): Traveling NADH and proton waves during oscillatory glycolysis *in vitro*. J. Biol. Chem. **271**, 627

Mori, Y., Nakamichi Y., Sekiguchi, T., Okazaki, N., Matsumura T., and Hanazaki, I. (1993): Photo-induction of cheimical oscillation in the Belousov-Zhabotinsky reaction under the flow condition. Chem. Phys. Lett. **211**, 56

Müller, S.C., Coullet, P. and Walgraef, D. (eds.): From Oscillations to Excitability, Chaos Focus Issue, Vol. 4 (AIP Publication, Woodbury , 1994)

Müller, S.C., Warda, A., and Zykov, V.S. (1995): Spiral waves in bounded excitable media. In: Modelling the Dynamics of Biological Systems, Mosekilde, E., Mouritsen, O.G. (eds.), Springer Series in Synergetics, Springer-Verlag, Berlin Heidelberg, p. 7.

Nagy-Ungvarai, Zs., Ungvarai, J., and Müller, S.C. (1993): Complexity in spiral wave dynamics. Chaos **3**, 15

Schmidt, B. (1995): Diploma thesis, Göttingen

Schütze, J., Steinbock, O., and Müller, S.C. (1992): Forced vortex interaction and annihilation in an active medium. Nature **356**, 45

Sevcikova, H. and Marek, M. (1983): Chemical waves in electric field. Physica **9D**, 140

Sevcikova, H., Marek, M., and Müller, S.C. (1992): The reversal and splitting of waves in an excitable medium caused by an electrical field. Science **257**, 951

Siegert, F. and Weijer, C. (1992): Three-dimensional scroll waves organize Dictyostelium slugs. Proc. Natl. Acad. Sci. USA **89**, 6433

Shinjyo, T., Nakagawa, Y., and Ueda, T. (1995): Hierarchic spatio-temporal dynamics in glycolysis. Physica D **84**, 212

Skinner, G.S. and Swinney, H.L. (1991): Periodic to quasiperiodic transition of chemical spiral rotation. Physica **48D**, 1

Steinbock, O. and Müller, S.C. (1993a): Multi-armed spirals in a light-controlled excitable reaction. Int. J. Bifurcation and Chaos **3**, 437

Steinbock, O., Zykov, V.S., and Müller, S.C. (1993b): Control of spiral-wave dynamics in active media by periodic modulation of excitability. Nature **366**, 322

Stock, D. and Müller, S.C. (1996): Three-dimensional reconstruction of scroll waves in the Belousov-Zhabotinsky reaction using optical tomography. Physica D, in press

Tyson, J.J. and Strogatz, S.H. (1991): The differential geometry of scroll waves. Int. J. Bifurcation and Chaos **1**, 723

Winfree, A.T. (1995): Persistent tangles of vortex rings in excitable media. Physica **D84**, 126

Winfree, A.T. (1987): When Time Breaks Down (Princeton University Press, Princeton)

Zykov, V.S., Mikhailov, A.S., and Müller, S.C. (1996): Spiral waves on a sphere: New computational results. In: Self-Organization in Activator-Inhibitor Systems, Engel, H., Niedernostheide, F.-J., Purwins, H.-G., and Schöll, E. (eds.), WET-Verlag, Berlin

Zykov, V.S., Steinbock, O., and Müller, S.C. (1994): External forcing of spiral waves. Chaos **4**, 509

Electric-Field-Induced Drift and Deformation of Spiral Waves in an Excitable Medium

O. Steinbock, J. Schütze, and S. C. Müller

Max-Planck-Institut für Ernährungsphysiologie, Rheinlanddamm 201, D-4600 Dortmund 1, Federal Republic of Germany

(Received 20 September 1991)

The dynamic behavior of spiral-shaped excitation patterns in the Belousov-Zhabotinskii reaction was investigated under the influence of externally applied direct current. Spiral centers drift towards the anode. The chirality of the spirals determines the direction of an additional perpendicular drift. A deformation of the Archimedian spiral shape was observed. Both effects were studied quantitatively and were reproduced in simulations with a simple reaction-diffusion model.

PACS numbers: 82.20.Mj, 66.30.Qa, 82.20.Wt

Spatiotemporal patterns formed in systems far from equilibrium have been investigated intensively in recent years. One of the most interesting and thoroughly studied systems remains the classical Belousov-Zhabotinskii (BZ) reaction [1], which is the oxidation of malonic acid by bromate in the presence of catalysts such as ferroin or cerium. Extended excitable systems such as thin layers of the BZ reaction exhibit patterns, such as rotating spirals or expanding trigger waves. In particular, the core region of spirals is a major focus of scientific interest [2]. For BZ media showing a sufficiently high excitability the core location remains stable in time; thus the spiral tip rotates around a circle. Remarkably, systems with low excitability show a different behavior: The spiral tip starts to meander [3], tracing out "floral" trajectories [4], but there are also experimental and numerical results showing more complex wandering of the tip along unpredictable traces [5]. Furthermore, Agladze, Davydov, and Mikhailov [6] and Mikhailov [7] suggested the possibility of controlled spiral drift by varying the excitability in time or space.

In this Letter we introduce a new technique with the goal of forcing spiral drift. This drift is caused by a small direct current, which influences the transport of ions. Sevcikova and Marek [8,9] studied this interaction in one-dimensional systems. They observed a speeding up of traveling waves towards the anode and a slowing down towards the cathode. Feeney, Schmidt, and Ortoleva [10] were the first who investigated the influence of electric fields on two-dimensional patterns in BZ media. These authors show that wave fronts can be broken or split by high electric currents.

Solution was prepared from distilled water and reagent grade chemicals and mixed with liquid agar (0.4%), which after solidification prevents hydrodynamic effects during the experiment. The final composition of the solution was 0.05M BrO_3^-, 0.05M malonic acid, 0.2M H_2SO_4, and $6.25\times10^{-4}M$ ferroin [$Fe(phen)_3SO_4$]. The mixture was placed in a flat, rectangular dish (71.6×21.0 mm^2) with a layer thickness of 3 mm. Under these conditions patterns persist for more than 2 h. In order to account for the Ohmic heating (σE^2), a cooling box controlled the temperature of the dish at 25 ± 1.0°C. A small glass-coated thermoelectric couple measured the temperature. The electrodes were placed parallel to the short edges of the dish (Fig. 1). Metal brackets closed the electric circuit, which was driven by a dc power supply fixing the current to an arbitrary strength (I=0–40 mA). The experimental pictures were taken by a charge-coupled-device video camera connected to a time lapse video recorder. For computational analysis the pictures were digitized with an image acquisition card (512×512 pixels, 8 bits gray level) and sent to a Convex-C201 computer.

Two different techniques contribute to the analysis of the experimental data. We first detected the traces of core drift by searching iteratively those pixel sites at which only very small gray level changes occur during one spiral period. This method takes advantage of the feature that the chemical activity inside the core region is very small [2]. The resulting coordinates of core location as a function of time were analyzed by linear regression. Second, we studied the spiral shape and its deformation by detecting that part of the wave profile which shows the strongest increase in intensity and calculating the corresponding polar coordinates (r,ϕ) with respect to the core center.

The analysis of drifting spiral tips reveals a surprising behavior: The electric field forces the cores to drift towards the anode, with an additional component perpendicular to the field vector. The direction of this perpendicular drift depends on the chirality of the spirals, as

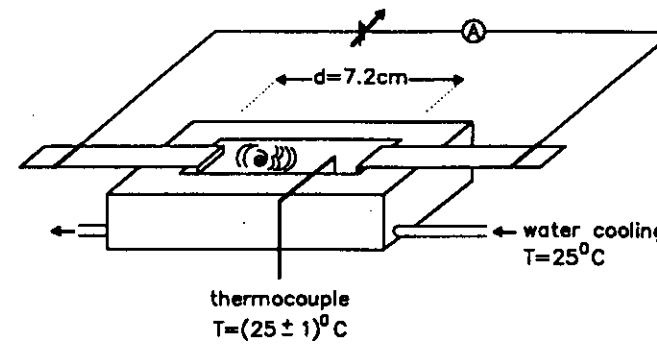

FIG. 1. Schematic representation of the experimental setup. Two K_2SO_4 soaked paper strips are used as planar electrodes in order to apply an electric current on a thin agar layer carrying the BZ solution. The excitation patterns were detected by a video camera with a BG filter (Schott).

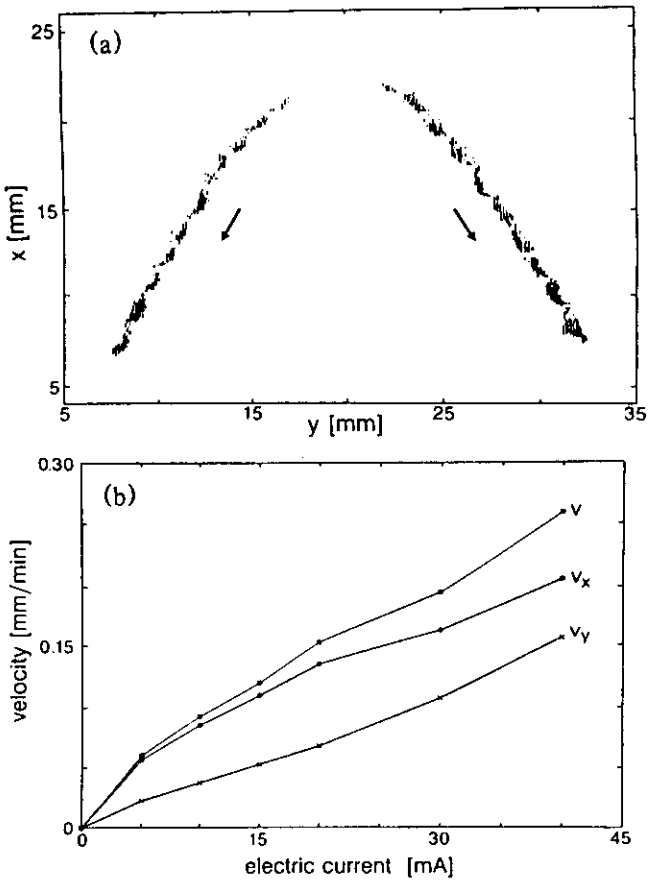

FIG. 2. (a) Core locations of two drifting spirals with different sense of rotation. Locations were estimated by detecting places of low-intensity changes. The applied electric current was $I=35.0$ mA, with the anode at the bottom of the graph. (b) Dependence of velocity of drifting cores on current. The velocity component v_x is parallel to the electric field; v_y is perpendicular. The chirality of a spiral determines the sign of v_y.

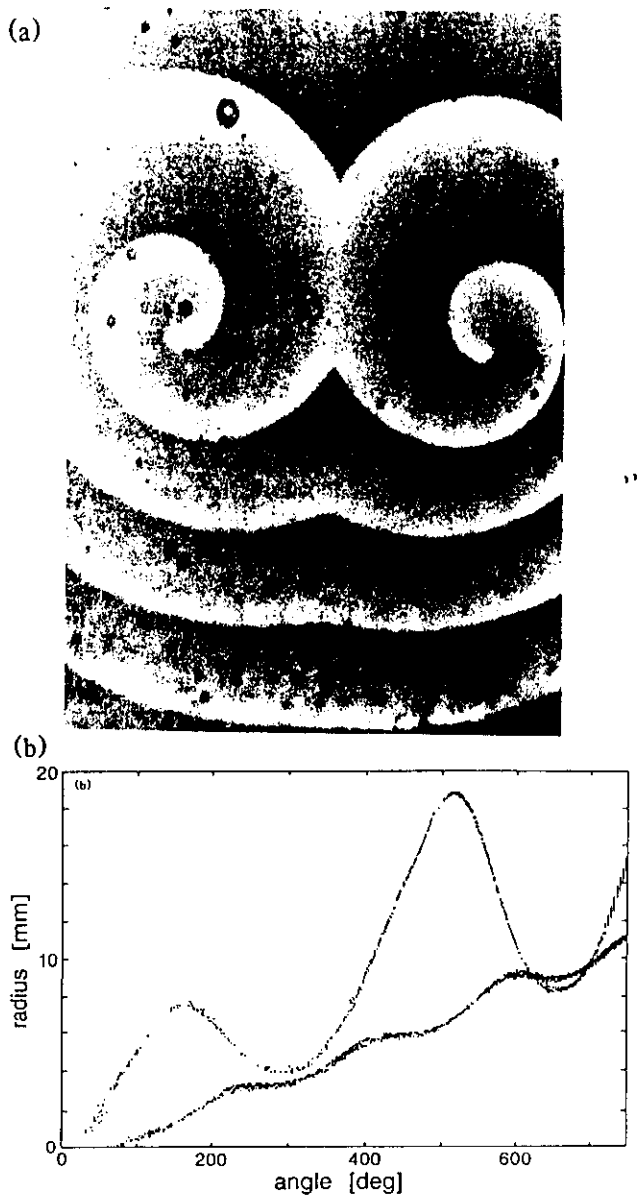

FIG. 3. (a) Image of deformed spiral patterns, with $I=35$ mA. (b) Polar coordinates of two spiral wave fronts with respect to their core center. The unperturbed spiral ($I=0$ mA) shows a linear (Archimedian) dependence. A current of 35.0 mA forces a deformation, which reaches its maximum in the back of the drift.

shown in Fig. 2(a). A current of $I=35.0$ mA, corresponding to approximately $E=5$ V/cm, shifted the spirals to the anode at the lower part of the plot. The left spiral, rotating clockwise, possesses an additional drift to the left side. The other spiral, rotating counterclockwise, drifts towards the right side. Switching off the current immediately stops the core drift. Changing the polarity of the field causes a core drift towards the initial position.

The velocity and angle of the drift strongly depend on the current strength. Higher electric current yields faster drift and larger angles. This dependence is shown in Fig. 2(b). With 0° for the field direction, the drift angle for $I=5$ mA is measured to be 22.5° and for $I=40$ mA is measured to be 37.2°. Quantitative experiments using higher currents are difficult because the large heat production causes higher and uncontrolled excitability. The shape of the core traces is linear only to a first approximation. In the later stage of the process we usually observed smaller angles.

The shape of unperturbed spirals in this recipe is very close to Archimedian [11]. A representation of its geometry in polar coordinates (r,ϕ) leads to a linear function: Moving along one whorl of the spiral (360°) causes a displacement of one wavelength. Figure 3(a) shows spirals that are deformed by a 35.0-mA current. A (r,ϕ) diagram of a deformed spiral is given in Fig. 3(b) including, for comparison, the shape without current. The deviation reaches its maximum in the back of the drift direction. The (r,ϕ) coordinates of the deformed spiral arm approach the unperturbed state near the drift angle.

For strong currents we found "filaments" with low curvature traveling without shape change and highly curved

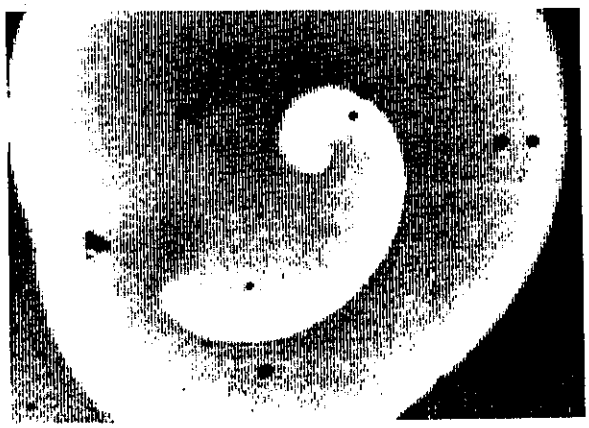

FIG. 4. Image of drifting spiral tips influenced by a 35-mA current. Most of the time the waves have the shape shown in the lower spiral, while cringing takes only a very short time (upper spiral).

wave ends that quickly cringe, as shown in the spiral pair of Fig. 4. The phase difference of rotation leads to an alternating occurrence of both types of structures at the two open ends. This phenomenon illustrates the main principle of forced spiral drift. In a first approximation, the action of the electric field on a wave front depends on the cosine of the angle θ between field vector and normal wave velocity. The motion of the unperturbed spiral tip which is rotating around a circular core region with constant frequency causes a linear increase of this angle. The electric field modulates the rotation frequency $\omega(\theta)$ and the absolute position of the tip, resulting in the observed behavior.

We suppose that the described phenomena are mainly due to a field-induced transport of the inhibitor Br^-. It should be noted that the temporal evolution of the bromide concentration is anticorrelated to that of the autocatalytic component $HBrO_2$. Effects of the external perturbation on the large ferroin complex might be less important.

A simple two-variable reaction-diffusion model can give insights into the mechanism of electric-field-induced drift and deformation, when the equation of the propagator variable u is modified by an additional convection term, as described by Schmidt and Ortoleva [12]:

$$\frac{\partial u}{\partial t} = D\Delta u + f(u,v) + ME\frac{\partial u}{\partial x}, \tag{1}$$

$$\frac{\partial v}{\partial t} = g(u,v), \tag{2}$$

with the diffusion coefficient D, the ion motility M, and the electric-field strength E. We used the nonlinear kinetic rate laws for excitable media suggested by Barkley [13].

By integrating this system of partial differential equations we found stable core positions for spirals without electric current. Nonzero values of E result in drifting

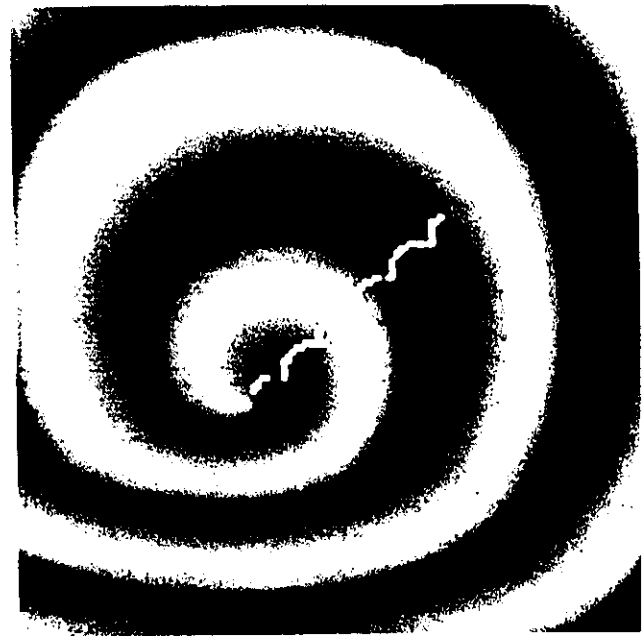

FIG. 5. Numerical simulation of a drifting and deformed spiral. The trace of the spiral core (bright dots) is superposed on the final spatial distribution of the variable v. In this example the value of ME/D was 0.35. Simulations were done by using a 150×150 grid point array.

spiral centers and deformation of the spiral shape. A typical example of both effects is shown in Fig. 5. In this simulation the value of ME/D was 0.35. The evolution of the intersection of the $u=0.50\pm0.02$ and $v=0.34\pm0.03$ level curves provided the trajectories of drifting spiral tips.

Detailed analysis of drift velocities reveals a monotonic dependence on the electric-field strength E [Fig. 6(a)]. The velocity component parallel to the field v_x and the corresponding drift angle show smaller increases for larger values of E. The angle seems to converge to approximately 60°. Figure 6(b) presents the polar coordinates of spiral wave fronts without convection and for $ME/D=0.35$. Without any electric field, we found only small wiggles in an overall linear dependence caused by the quadratic geometry of the grid cells and the simple five-point calculation of the Laplacian. For strong electric fields, there are significant deviations from the Archimedian shape, as found in the experiment.

All computational results are in good qualitative agreement with the experimental observations. Furthermore, such numerical simulations help to study the effects of stronger current under controlled conditions. The simplicity of the model used indicates that the phenomenon of drifting spirals is a common property of excitable media in which long distance transport takes place.

Numerical simulations reveal that only waves propagating into a completely recovered region show a linear dependence of wave velocity on electric-field strength. Drift and deformation appear to be strongly influenced by

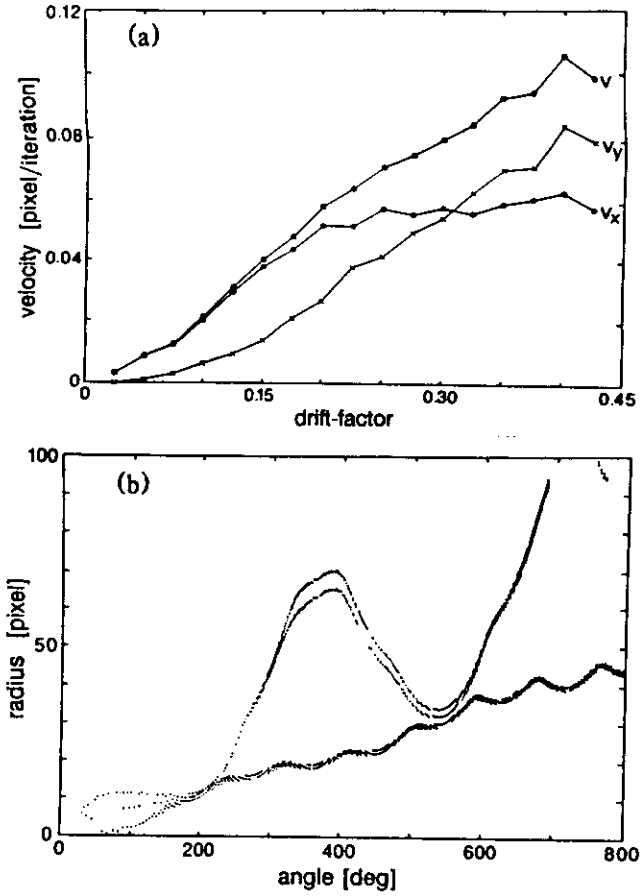

FIG. 6. (a) Numerically simulated drift velocities v as a function of drift factor ME/D. v_x describes the velocity component in the x direction (direction of the electric field); v_y is the perpendicular component. (b) Polar coordinates of two simulated spiral waves with respect to their core center. Increasing the value of ME/D leads to a strong deformation of the unperturbed spiral shape (compare Fig. 3).

the dispersion relation [14] of the system and by the characteristic action of the electric field.

We recently have obtained direct experimental evidence for the annihilation of spiral pairs that collide under the influence of electric fields. Furthermore, we observed a temporal interaction of spiral centers trying to surround each other in order to continue their own unperturbed drift [15]. The experimental and computational techniques presented are important new tools for the field of pattern dynamics in excitable systems. These results will probably simplify the explanation of compound tip motion and will reveal new insights in the structure and stability of spiral cores.

We thank Zs. Nagy-Ungvarai, H. Sevcikova, and A. Pertsov for helpful discussions.

[1] *Oscillations and Travelling Waves in Chemical Systems*, edited by R. J. Field and M. Burger (Wiley, New York, 1985).
[2] S. C. Müller, T. Plesser, and B. Hess, Science **230**, 661 (1985).
[3] G. S. Skinner and H. L. Swinney, Physica (Amsterdam) **48D**, 1 (1991).
[4] W. Jahnke, W. E. Skaggs, and A. T. Winfree, J. Phys. Chem. **93**, 740 (1989).
[5] M. Gerhardt, H. Schuster, and J. J. Tyson, Physica (Amsterdam) **46D**, 392 (1990).
[6] K. I. Agladze, V. A. Davydov, and A. S. Mikhailov, Pis'ma Zh. Eksp. Teor. Fiz. **45**, 601 (1987) [JETP Lett. **45**, 767 (1987)].
[7] A. S. Mikhailov, *Foundations of Synergetics—Distributed Active Systems* (Springer-Verlag, Berlin, Heidelberg, 1990).
[8] H. Sevcikova and M. Marek, Physica (Amsterdam) **9D**, 140 (1983).
[9] H. Sevcikova and M. Marek, Physica (Amsterdam) **21D**, 61 (1986).
[10] R. Feeney, S. L. Schmidt, and P. Ortoleva, Physica (Amsterdam) **2D**, 536 (1981).
[11] S. C. Müller, Th. Plesser, and B. Hess, Physica (Amsterdam) **24D**, 87 (1987).
[12] S. Schmidt and P. Ortoleva, J. Chem. Phys. **67**, 3771 (1977).
[13] D. Barkley, Physica (Amsterdam) **49D**, 61 (1991).
[14] J. D. Dockery, J. P. Keener, and J. J. Tyson, Physica (Amsterdam) **30D**, 177 (1988).
[15] J. Schütze, O. Steinbock, and S. C. Müller (to be published).

Control of spiral-wave dynamics in active media by periodic modulation of excitability

Oliver Steinbock, Vladimir Zykov* & Stefan C. Müller

Max-Planck-Institut für molekulare Physiologie, Rheinlanddamm 201, D-44139 Dortmund 1, Germany

EXCITABLE media exhibit a wide variety of geometrically complex spatio-temporal patterns, perhaps the most striking of which are rotating spiral waves. Spiral waves have now been observed in many excitable systems, including heart muscle[1], aggregating slime-mould cells[2], retinae[3], CO oxidation on platinum[4] and oscillatory chemical systems such as the Belousov–Zhabotinsky (BZ) reaction[5,6]. In the last case, the spiral cores trace out circular or hypocycloidal trajectories, depending on the specific reaction conditions[7–9]. In addition, if the excitability of the BZ reaction is light-sensitive[10–13], constant illumination has been shown to influence the dynamics of spiral waves[14,15]. Here we investigate the effect of illumination that is periodically modulated in time. We find that, for a single set of reaction conditions, the motion of the spiral cores can be forced to describe a wide range of open and closed hypocycloidal trajectories, in phase with the applied modulation frequency. Numerical simulations using a modified version of the Oregonator model[16,17] of the BZ reaction reproduce this behaviour. We suggest that the modulation of excitability with weak external forces might be used as a means for controlling the dynamics of other excitable media.

In the light sensitive BZ reaction[10,11], a ruthenium-bipyridyl complex is used to promote the autocatalytic production of the reaction activator $HBrO_2$. This only occurs when the complex is in its reduced, and electronically unexcited state. If the ruthenium complex is photochemically excited, it slowly catalyses the production of the inhibitor species, bromide. Thus externally applied illumination suppresses the excitability of the medium (for instance, it decreases the propagation velocity of excitation waves) and allows control of spiral wave parameters[12–15].

In our experiments $Ru(bpy)_3^{2+}$ (4 mM) was immobilized in a silica-gel matrix[18] (thickness 0.7 mm, diameter 7 cm). The reactants and their concentrations (disregarding bromination of malonic acid) were; NaBr (0.09 M), $NaBrO_3$ (0.19 M), malonic acid (0.17 M) and H_2SO_4 (0.35 M). The temperature was kept constant at 23 ± 1 °C. White light (halogen lamp, 150 W) illuminating the entire observation area was polarized by a rotating polarization filter and applied to the active medium through a tilted glass plate. Because of the rotation of the polarization vector the intensity of the reflected light was modulated sinusoidally with time (0.49–1.36 mW cm^{-2}). The transmitted light was detected by CCD (charge-coupled device) camera (Hamamatsu C3077) at 490 nm, stored on a video recorder and finally digitized by an image-acquisition card.

We created a spiral wave by using a thin laser beam to break a propagating circular wave (this creates two spirals) and moving one of the open ends to the boundary of the dish[19]. The temporal trace of the wave tip was detected visually with a reticle in digitized images. Figure 1 shows a snapshot of the created spiral wave (constant light intensity, 0.93 mW cm^{-2}) with the overlaid trajectory of its tip. The trajectory is almost a five-lobed hypocycloid with the wave period $T_0 = 24.5$ s at the centre of the meandering pattern. The change in the stationary intensity level of illumination in the range from 0.49 to 1.36 mW cm^{-2} leads only to small variations of the spatio-temporal parameters of the spiral wave. For the minimum and maximum intensities applied here, we observed four- and six-lobed trajectories, respectively.

Periodic modulation of the applied light intensity within the same range causes dramatic changes in the dynamics of spiral rotation. The small variations of the trajectory shape that occur during each period of the modulation accumulate with time. As a result, the modulation forces the tip to follow trajectories that

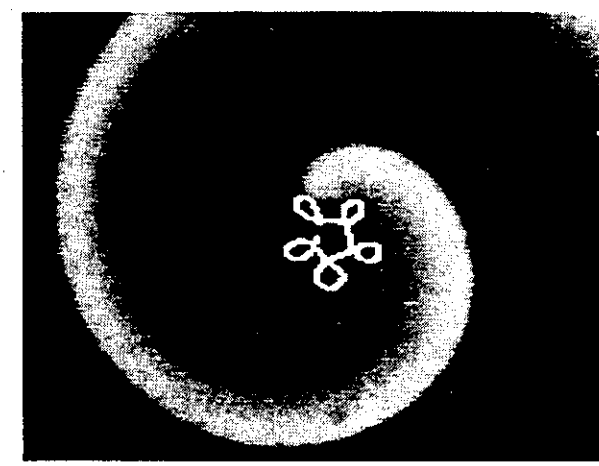

FIG. 1 Spiral wave in the ruthenium-catalysed BZ reaction at a steady level of light intensity (0.93 mW cm^{-2}). In the experiment bright bands are green, and dark bands are orange. The tip trajectory (overlaid white curve) is similar to a hypocycloid. Image size 3.8 × 3.0 mm.

* Permanent address: Institute of Control Sciences, Moscow, Russia.

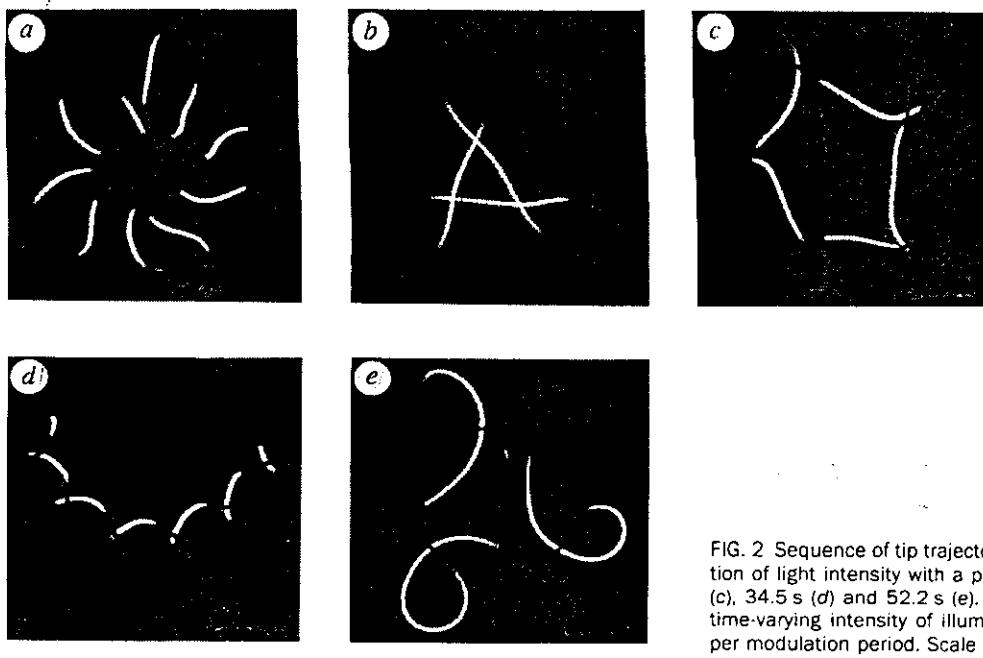

FIG. 2 Sequence of tip trajectories measured under sinusoidal modulation of light intensity with a period T_m of: 17.0 s (*a*), 26.2 s (*b*), 30.4 s (*c*), 34.5 s (*d*) and 52.2 s (*e*). The shading of the traces is due to the time-varying intensity of illumination and shows the number of lobes per modulation period. Scale bar, 0.2 mm.

differ significantly from those observed at constant intensities. The shape of trajectories depends strongly on the modulation period T_m (see Fig. 2). The trajectories of Fig. 2*b–d* are members of an entrainment band ($T_m \approx 20$–35 s) of closed hypocycloids with one lobe corresponding to one external period. The number of lobes continuously increases from 3 to more than 12 with increasing values of T_m. Figure 2*a* shows a deformed five-lobed pattern with one lobe described during two modulation periods. Figure 2*e* depicts a surprising trajectory with alternating distances between neighbouring lobes. In this small frequency range the spiral tip describes a pair of lobes during one external modulation. For modulation periods between those of Fig. 2*d* and *e* we observed irregular motion with epicyclic segments of the trajectories. In all examples of Fig. 2 the tip motion is synchronized by the external rhythm.

We complemented the experiments by numerical simulations of the observed process of synchronization. For this purpose we used an Oregonator model[16,17], which was extended by a term ϕ describing the light-induced bromide production[11].

$$\frac{\partial u}{\partial t} = \Delta u + \frac{1}{\varepsilon}\left[u - u^2 - (fv + \phi)\frac{u-q}{u+q} \right]$$

$$\frac{\partial v}{\partial t} = u - v$$

The variables u and v describe the time–space evolution of the $HBrO_2$ and catalyst concentration, respectively. While the parameters $\varepsilon = 0.05$, $q = 0.002$ and $f = 2.0$ are constant, the term $\phi(t) = 0.01 + A \sin(2\pi t/T_m)$ describes the periodic modulation of bromide production, and hence excitability.

In our calculations we studied the trajectories of the spiral tip for different values of the modulation period T_m and amplitude A. The unperturbed trajectory ($A = 0$) is similar to a five-lobed hypocycloid (see Fig. 1) and the excitation period measured at the symmetry centre is $T_0 = 2.8$. Our calculations show that the motion of the spiral tip can be synchronized by external modulation. In Fig. 3 the most pronounced entrainment bands are shown (labelled 1:3, 1:2, 1:1 and 2:1), with the broadest band observed around the modulation period $T_m = T_0$. For this band one loop is completed during one modulation period. Each modulation period for the furthest right (2:1) band in Fig. 3 contains two loops. On the left side of the diagram two bands (1:3 and 1:2) are shown which correspond to five-lobed trajectories but deformed with respect to the unperturbed one. Each loop of these meandering pictures is described during two (1:2 band) or three modulation periods (1:3 band). Within the entrainment bands the tip trajectory is sometimes rather complex but regular, in that the motion is still phase-locked. Between the bands, irregular behaviour apparently dominates. The simulation results for $A = 0.005$ are in good qualitative agreement with the experimental data given in Fig. 2. One can see the wide entrainment band ($T_m \approx T_0$) in which the lobe number increases from three up to infinity (as in Fig. 2*b–d*), the deformed five-lobed trajectory for $T_m \approx T_0/2$ (as in Fig. 2*a*) and characteristic pictures with pairs of petals for $T_m \approx 2 \times T_0$ (see Fig. 2*e*).

The nature of the described synchronization phenomenon is similar to entrainment in different kinds of oscillating systems in nonlinear physics[20] or chronobiology[21], but cannot be reduced to the case of zero spatial dimension. The resulting family of very unusual spatio-temporal patterns, including the transition from localized to infinite motion, has no close analogies with

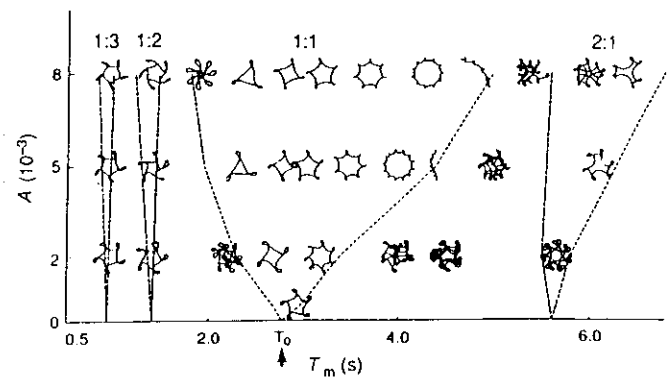

FIG. 3 Tip trajectories calculated as a response to sinusoidal modulation of bromide production. Trajectories (not to scale) are shown in the plane spanned by amplitude A and period T_m of modulation. Dashed lines indicate boundaries of entrainment bands related to different ratios $n:m$, where n is the number of lobes per m periods of the modulation. The vertical arrow on the x axis shows T_0, the intrinsic period of the unperturbed meandering spiral.

other examples of entrainment. The observed effects also differ essentially from the resonance drift induced by periodic forcing of an active medium[12] which occurs without synchronization and leads to displacement of the spiral-wave core as a whole, without the pronounced deformations of the tip trajectory[22] characteristic of the described phenomenon. This new way to deform and translate a spiral wave by controlling excitability with even weak external forces could ultimately prove relevant to our understanding of pattern formation in the early stages of morphogenesis[2], or to the origin and possible control of abnormalities of heart rhythm[1]. □

Received 13 May; accepted 1 October 1993.

1. Davidenko, J. M., Pertsov, A. V., Salomonsz, R., Baxter, W. & Jalife, J. *Nature* **355,** 349–351 (1992).
2. Siegert, F. & Weijer, C. *J. Cell Sci.* **93,** 325–335 (1989).
3. Gorelova, N. A. & Bures, J. *J. Neurobiol.* **14,** 353–363 (1983).
4. Jakubith, S., Rotermund, H. H., Engel, W., von Oertzen, A. & Erth, G. *Phys. Rev. Lett.* **65,** 3013–3016 (1990).
5. Winfree, A. T. *Science* **175,** 634–636 (1972).
6. Field, R. J. & Burger, M. (eds) *Oscillations and Traveling Waves in Chemical Systems* (Wiley, New York, 1985).
7. Jahnke, W., Skaggs, W. E. & Winfree, A. T. *J. phys. Chem.* **93,** 740–749 (1989).
8. Plesser, Th., Müller, S. C. & Hess, B. *J. phys. Chem.* **94,** 7501–7507 (1990).
9. Skinner, G. S. & Swinney, H. L. *Physica* D**48,** 1–16 (1991).
10. Kuhnert, L. *Naturwissenschaften* **73,** 96–97 (1986).
11. Krug, H.-J., Pohlmann, L. & Kuhnert, L. *J. phys. Chem.* **94,** 4862–4866 (1990).
12. Agladze, K. I., Davydov, V. A. & Mikhailov, A. S. *JETP Lett.* **45,** 767–770 (1987).
13. Kuhnert, L., Agladze, K. I. & Krinsky, V. I. *Nature* **337,** 244–247 (1989).
14. Markus, M., Nagy-Ungvarai & Hess, B. *Science* **257,** 225–228 (1992).
15. Braune, M. & Engel, H. *Chem. Phys. Lett.* (in the press).
16. Field, R. J. & Noyes, R. M. *J. phys. Chem.* **60,** 1877–1884 (1974).
17. Jahnke, W. & Winfree, A. T. *Int. J. Bifurcation and Chaos* **1,** 445–466 (1991).
18. Yamaguchi, T., Kuhnert, L., Nagy-Ungvarai, Zs., Müller, S. C. & Hess, B. *J. phys. Chem.* **95,** 5831–5837 (1991).
19. Steinbock, O. & Müller, S. C. *Physica* A**188,** 61–67 (1992).
20. Schuster, H. G. *Deterministic Chaos* (VCH, Weinheim, 1989).
21. Hildebraudt, G., Gutenbrunner, Ch. & Moog, R. (eds) *Chronobiology and Chronomedicine* (Peter Lang, Frankfurt, 1922).
22. Davydov, V. A., Zykov, V. S. & Mikhailov, A. S. *Soviet. Phys. Usp.* **34,** 665–684 (1991).

ACKNOWLEDGEMENTS. This work was supported by the European Community (DG XII) and the Boehringer Ingelheim Fonds, Stuttgart.

Feedback-Controlled Dynamics of Meandering Spiral Waves

S. Grill, V. S. Zykov, and S. C. Müller

Max-Planck-Institut für Molekulare Physiologie, D-44139 Dortmund, Germany

(Received 10 May 1995)

The effect of a sequence of short light impulses forcing a meandering spiral wave in the Belousov-Zhabotinsky reaction is investigated. Each stimulus is applied at a moment that corresponds to the passage of the wave front through a particular measuring point of the excitable medium. It is shown that the introduction of such a feedback results in two new dynamical regimes, named entrainment and resonance attractors. For both regimes the trajectory of the spiral wave tip has a symmetry center located at the measuring point. The experimental results are consistent with numerical simulations performed with the two-component Oregonator model.

PACS numbers: 82.80.Ch, 05.70.Ln, 82.20.Wt, 87.90.+y

Spiral waves of excitation belong to the most intriguing spatiotemporal patterns in nonequilibrium reaction-diffusion systems. They are observed in such diverse systems as cardiac muscle tissue [1], aggregating slime-mold cells [2], CO oxidation on platinum surfaces [3], and the chemical Belousov-Zhabotinsky (BZ) reaction [4–6]. Control of these dynamic regimes is important in many applications including the prevention of cardiac arrhythmia [1]. The BZ reaction turned out to be the most suitable laboratory system to study the dynamics of spiral waves and to elaborate adequate means of control. If the light-sensitive catalyst $Ru(bpy)_3^{2+}$ is used the dynamics of the system can be effectively controlled by external illumination [7–11]. For instance, under constant illumination the shape of the trajectory of a spiral wave tip strongly depends on the applied light intensity [12]. Under harmonic modulation of the uniform illumination, a synchronization of the movement of the spiral tip by the external forcing within entrainment bands [13] and a resonance drift of the spiral core are observed [14,15].

In this work we used the light-sensitive BZ reaction as a tool to study the effect of a feedback-controlled forcing which has been shown to be very essential for oscillatory and wave processes in active media [16,17]. For this purpose a spiral wave rotating in the BZ solution was forced by a sequence of short "light pulses," and the time instant for applying each stimulus was determined by the activity level measured at a particular point of the system.

The experimental setup included a petri dish (diameter 7 cm) containing a thin layer (0.7 mm) of silica gel with 4.2 m*M* $Ru(bpy)_3^{2+}$ [18]. The BZ solution (18 ml) was poured onto this gel, and after chemical equilibrium was established the concentrations of the reactants (disregarding the bromination of malonic acid) were 0.2*M* $NaBrO_3$, 0.17*M* malonic acid, 0.39*M* H_2SO_4, and 0.09*M* NaBr. The experiments were carried out at a temperature of 23 ± 1 °C.

White observation light (halogen lamp, 250 W), which was used simultaneously to control the excitability, was applied to the petri dish through two polarization filters. One of these could be rotated by a computer-controlled stepper motor. Programmed rotation of the filter generated any desired function of light intensity in the range between 0.01 and 2.22 mW/cm^2. In our case the permanent "background intensity" of the illumination was fixed to 0.5 mW/cm^2. The stimulating light pulse (if triggered) was a short (5 s) increase of the global illumination intensity up to 1.5 mW/cm^2. Each intensity jump corresponded to 150 single steps of the stepper motor and took 0.54 s.

A charged-coupled device camera detected the transmitted light at 490 nm, which is near the maximum difference of absorption between the oxidized and reduced form of the catalyst (at 460 nm). The observed pictures of the catalyst concentration waves were digitized by an image acquisition card, analyzed on-line, and also stored on a video recorder [9].

To start an experiment a spiral wave was created in the center of the dish by breaking a circular wave front with a thin laser beam (diameter 1 mm) and shifting one of the two originating open ends to the boundary of the dish [9,10]. The remaining open end evolved into a single, unperturbed spiral wave. Its tip was determined automatically as the intersection of two overlaid contour lines of the spiral wave extracted from two consecutive frames (time step 1.44 s).

At a constant intensity of 0.5 mW/cm^2 the trajectory of the tip is approximately a four-lobed hypocycloid (dashed line in Fig. 1) with a wave period $T_\infty \approx 33$ s at a point far away from the tip and remains so for at least 2 h. An applied single light impulse deforms the trajectory. Nevertheless, the trajectory of the tip stabilizes soon after the stimulus and forms a similar four-lobed hypocycloid which is shifted and rotated with respect to the initial one (solid line in Fig. 1). In addition, the phase of the angular velocity, which is a periodical function, is shifted in time. All the parameters describing the effect of a single stimulus on the spiral wave dynamics depend on the phase of the tip motion at the instant when the stimulus is applied.

To realize the desired feedback mechanism the intensity of the transmitted light at a particular measuring point is determined on-line with a time interval of 0.02 s. Every time a wave front reaches the measuring point a

 0031-9007/95/75(18)/3368(4)$06.00

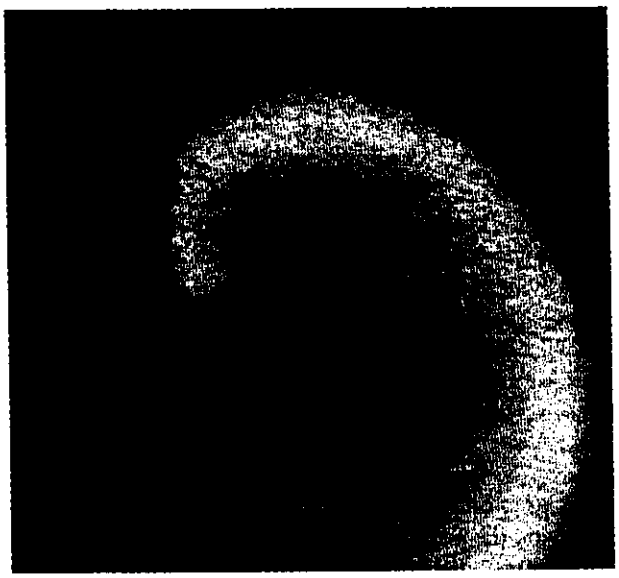

FIG. 1. The trajectory of the spiral wave tip observed for the constant background intensity of the illumination before (dashed line) and after (solid line) the application of the single light pulse. An intermediate position of the spiral wave is shown. Scale bar: 0.5 mm.

single stimulus is triggered immediately or with a certain time delay τ after the wave-front passage. When the feedback mechanism is switched on, the spiral is forced by a sequence of short impulses. The influence of each stimulus is overlayed with the effect of all the previous ones, which leads to the observation of two new regimes shown in Fig. 2.

If the measuring point is placed close to the center of the unperturbed trajectory, the feedback results in a synchronization of the tip motion by the external stimuli [see Fig. 2(a)]. After some transient process, the spiral tip approaches an asymptotic trajectory with a symmetry center located at the measuring point. In this case the spiral is forced by a periodic sequence of short stimuli leading to a deformation (as a rule to a blow-up) of the trajectory. Nevertheless, the distance between the tip position and the measuring point remains on the order of the size of one loop. The period of the light pulses is exactly the time during which one loop of the trajectory is described. Consequently, each stimulus is applied at the same phase of each loop.

If the measuring point is placed rather far from the initial trajectory, one observes a quite different evolution of the trajectory, as illustrated in Fig. 2(b). The tip of the spiral wave approaches a stable trajectory, which looks like a drift of the four-lobed hypocycloid along a large circle. The center of this circle coincides again with the measuring point. A significant difference to the former regime: The sense of the core rotation around the measuring point is opposite, the sequence of the stimuli is not exactly periodical, and the stimuli are applied at different phases of the lobes. The average period is larger than in the first case.

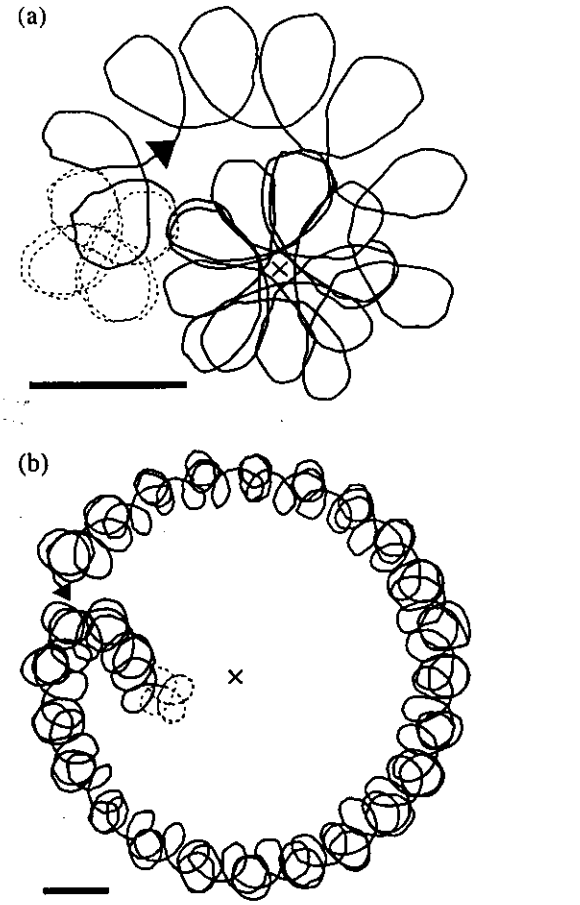

FIG. 2. Two attractors observed in the light-sensitive BZ reaction forced by a sequence of short light pulses applied at every moment when a wave front passes through the measuring point (+). The distance between the center of the unperturbed trajectory (dashed line) and the measuring point was (a) 0.49 mm, (b) 0.57 mm. Scale bars: 0.5 mm.

Both asymptotic trajectories are stable with respect to a small shift of the measuring point and can be considered as attractors for the studied dynamical system including a feedback.

So far, the experiments described above were performed without any artificial time delay τ in the feedback loop. We also investigated the role of a delay between the registration of a wave front at the measuring point and the triggering of the stimulus. We found that the synchronization also occurs if the delay is small with respect to the period of one loop [Fig. 3(a)]. The diameter of the synchronized trajectory increases with the delay [compare Figs. 1(a) and 3(a)]. This growth of diameter is accompanied by an increase of the number of the loops in the pattern. If the delay reaches a certain value, the synchronization breaks down, and only the regime of the drift around the measuring point is observed [Fig. 3(b)].

We complemented the experiments by numerical simulations of the observed phenomena. For this purpose we used an extension of the Oregonator model [19,20], which includes an additional term ϕ describing the light-induced

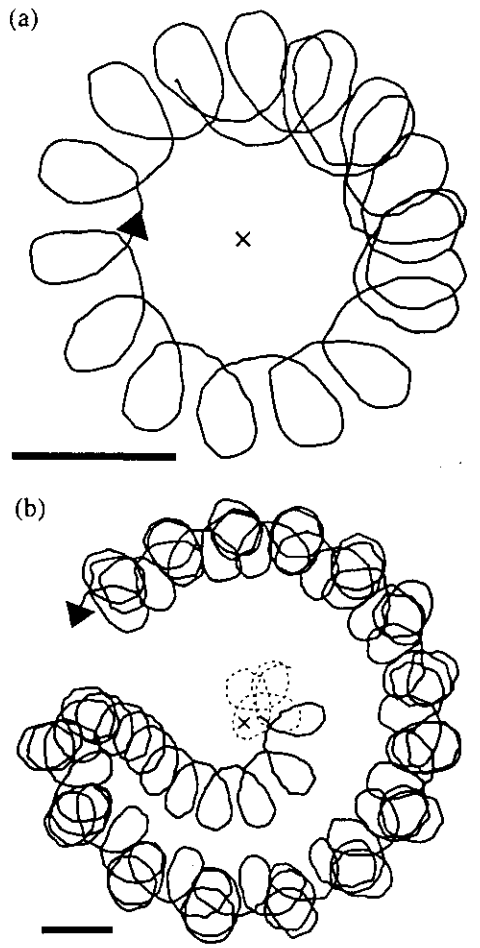

FIG. 3. Tip trajectories measured in the light-sensitive BZ reaction for different values of the time delay τ in the feedback loop: (a) $\tau = 5$ s and (b) $\tau = 7$ s. Scale bars: 0.5 mm.

bromide production [13,14].

$$\frac{\partial u}{\partial t} = \nabla^2 u + \frac{1}{\epsilon}\left[u - u^2 - (fv + \phi)\frac{u - q}{u + q}\right], \quad \text{(1a)}$$

$$\frac{\partial v}{\partial t} = u - v. \quad \text{(1b)}$$

The variables u and v describe the concentrations of the autocatalytic species $HBrO_2$ and the catalyst, respectively. The parameters $\epsilon = 0.05$, $q = 0.002$, and $f = 2.0$ were fixed. The term $\phi = \phi(t)$ describes an additional bromide production induced by the external illumination of the system. It consists of a sequence of impulses with amplitude A and duration D that are applied with a time delay τ after the passage of the wave fronts through a particular measuring point. These impulses are added to a background flow $\phi_0 = 0.01$.

In our calculations we fixed the duration to $D = 0.3$ and studied the trajectories of the spiral wave tip for different values of the amplitude A and the delay τ. The computations were performed by the explicit Euler method, using the five-point approximation of the Laplacian on a 380×380 array with a grid spacing $\Delta x = 0.1$ and time steps $\Delta t = 0.001$.

A single spiral was induced by a special choice of initial conditions for the system (1). For zero amplitude A of the stimulus one can observe the unperturbed trajectory, which is close to a five-lobed hypocycloid with a wave period $T_\infty = 3.6$ Oregonator time units measured far away from the symmetry center.

If the center of the unperturbed spiral wave is located rather close to the measuring point, it is attracted to this new position after same transient process [Fig. 4(a)]. If this initial distance is large enough, one can observe an evolution to another attractor: The center of the unperturbed hypocycloid moves and describes a big circle around the measuring point [Fig. 4(b)].

Increasing the delay τ results in a large number of lobes for the first type of attractor [compare Figs. 4(a) and 5(a)]. The synchronization breaks down for a rather big delay, and the system then tends to the second attractor [Fig. 5(b)]. The observed deformation of the unperturbed trajectory becomes more pronounced if a stimulus with higher amplitude A is applied. The radius of the big circle which characterizes the trajectory for the second type of attractor decreases with the time delay τ in the feedback

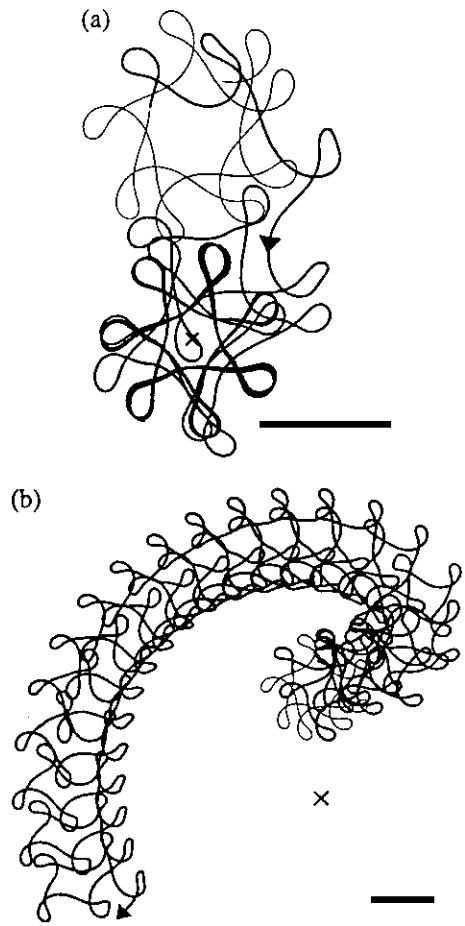

FIG. 4. Two attractors computed for the model (1) with $A = 0.01$ and $\tau = 0.5$. The distance between the center of the unperturbed trajectory (thin line) and the measuring point was (a) 6 Oregonator space units (su), (b) 7 su. Scale bars: 4 su.

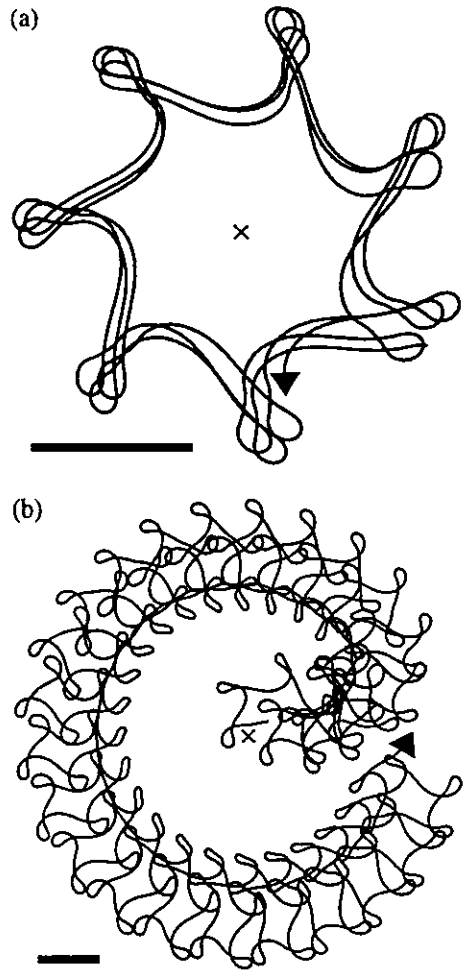

FIG. 5. Tip trajectories computed for the model (1) with $A = 0.01$ and different values of the time delay τ in the feedback loop: (a) $\tau = 0.8$ and (b) $\tau = 1.5$. Scale bars: 4 Oregonator space units.

loop. The increase of the amplitude A results in an increase of the drift velocity along this circle but does not influence its radius.

Thus, the numerical simulations very well confirm the existence of the two kinds of attractors observed in the experiments with the BZ reaction controlled by a feedback mechanism. The nature of these attractors becomes more clear if one takes into account earlier results obtained for the external forcing of spiral waves [13,14]. If the measuring point is located in the symmetry center of a meandering trajectory, the period of the stimuli is exactly equal to the period of one lobe of the trajectory, and the phase of the applied stimulus is the same for each lobe. We call this regime "entrainment attractor" because it exhibits the basic properties of frequency entrainment as it occurs in similar systems with a periodic modulation of the excitability, but without feedback [13,14]. Either way, the increase of the number of lobes with the time delay can be interpreted as an effect of the phase of the applied stimulus and corresponds to the variety of the trajectories induced by different phase relationships within an entrainment band [14].

In the second case the measuring point is far away from the tip trajectory. A different period of excitation ($T \approx T_\infty$) is registered at the measuring point. As observed earlier for the system without feedback [14], the external forcing of the spiral wave with such a period results in a so-called resonance drift. For this reason we call this regime "resonance attractor." A similar regime occurs in the case of nonmeandering spiral waves [17]. The location of a separatrix between these two attractors was determined very roughly yet. It depends on the amplitude and the delay of the stimulus as well as on the initial orientation of the unperturbed pattern.

Both these attractors are stable with respect to a small shift of the measuring point. Moreover, the center of the meandering pattern follows any slow displacement of this particular point. Hence, the described feedback mechanism yields a powerful means to control the position of a spiral wave using only comparatively small global perturbations.

V. S. Z. acknowledges support from the WE-Heraeus-Stiftung, Hanau.

[1] J. M. Davidenko, A. V. Pertsov, R. Salamonz, W. Baxter, and J. Jalife, Nature (London) **355**, 349 (1992).
[2] G. Gerish, Naturwissenschaften **58**, 430 (1983).
[3] S. Jakubith, H. H. Rotermund, W. Engel, A. von Oertzen, and G. Ertl, Phys. Rev. Lett. **65**, 3013 (1990).
[4] A. N. Zaikin and A. M. Zhabotinsky, Nature (London) **225**, 535 (1970).
[5] A. T. Winfree, Science **175**, 634 (1972).
[6] Th. Plesser, S. C. Müller, and B. Hess, J. Phys. Chem. **94**, 7501 (1990).
[7] L. Kuhnert, Naturwissenschaften **73**, 96 (1986).
[8] K. I. Agladze, V. A. Davydov, and A. S. Mikhailov, JETP Lett. **45**, 767 (1987).
[9] O. Steinbock and S. C. Müller, Physica (Amsterdam) **188A**, 61 (1992).
[10] O. Steinbock and S. C. Müller, Phys. Rev. E **47**, 1506 (1993).
[11] M. Markus, Zs. Nagy-Ungvarai, and B. Hess, Science **257**, 225 (1992).
[12] M. Braune and H. Engel, Chem. Phys. Lett. **204**, 257 (1993).
[13] O. Steinbock, V. S. Zykov, and S. C. Müller, Nature (London) **366**, 322 (1993).
[14] V. S. Zykov, O. Steinbock, and S. C. Müller, Chaos **4**(3), 509 (1994).
[15] M. Braune, A. Schrader, and H. Engel, Chem. Phys. Lett. **222**, 358 (1994).
[16] G. Veser, F. Mertens, A. S. Mikhailov, and R. Imbihl, Phys. Rev. Lett. **71**, 935 (1993).
[17] V. N. Biktashev and A. V. Holden, J. Theor. Biol. **169**, 101 (1994).
[18] T. Yamaguchi, L. Kuhnert, Zs. Nagy-Ungvarai, S. C. Müller, and B. Hess, J. Phys. Chem. **95**, 5831 (1991).
[19] R. J. Field and R. M. J. Noyes, Chem. Phys. **60**(5), 1877 (1974).
[20] W. Jahnke and A. T. Winfree, Int. J. Bifurcation Chaos **1**, 445 (1991).

Spatial Attractors in Aggregation Patterns of *Dictyostelium discoideum*

Oliver Steinbock* and Stefan C. Müller

Max-Planck-Institut für molekulare Physiologie, Rheinlanddamm 201,
D-44139 Dortmund, Bundesrepublik Deutschland

Z. Naturforsch. **50c**, 275–281 (1995); received August 2, 1994/January 17, 1995

Chemotaxis, Excitable Media, Reaction-Diffusion Coupling, Spiral Waves

Chemotactic cell motion in aggregation patterns of the slime mould *Dictyostelium discoideum* is analyzed by a computerized cross-correlation method. In this excitable medium the movement of amoebae is selforganized by signals of cAMP that propagate as rotating spirals or expanding concentric circles (target patterns). A vortex-like rotation of cells is found close to the core of spiral waves, with a maximum velocity of 15 μm/min. Cell motion and spiral tip orbiting follow an opposite sense of rotation. The calculation of streamlines of the most probable trajectories reveals the exsitence of a closed curve (radius ≈ 130 μm) corresponding to the boundary of the spiral core. This spatial-limit cycle attracts the amoebae on rotational paths and leads to the formation of a cell-free disk in the centre of the pattern. In contrast, pacemakers of target patterns organize cell movement in a radial, star-shaped motion, leading directly to the formation of central mounds.

Introduction

The slime mould *Dictyostelium discoideum* is well suited for the study of cellular communication and a widely investigated example of selforganizing nonlinear systems. Single amoebae of this myxomycete aggregate to form a pseudoplasmodium. Subsequently, they differentiate to form a fruiting body bearing spores (Loomis, 1982). The depletion of their food source serves as signal to trigger the onset of the corresponding developmental cycle. The aggregation is coordinated and organized by traveling waves of cyclic adenosinemonophosphate (cAMP) (Tomchik and Devreotes, 1981). During this phase the majority of the population rests in an excitable state, while other cell groups serve as periodic pacemakers by producing cAMP according to an oscillatory mechanism. By means of diffusion their neighborhood becomes excited and relays the biochemical signal. Propagating waves result which show, in general, the geometry of concentric circles (target patterns) or rotating spirals (Fig. 1). These structures are usually investigated by darkfield-photography (Siegert and Weijer, 1989; Foerster *et al.*, 1990).

The aggregation patterns formed in this living excitable system are similar to patterns observed in the chemical Belousov-Zhabotinsky (BZ) reaction (Winfree, 1972), during the oxidation of carbonmonoxyde on platinum crystals (Jakubith *et al.*, 1990), or propagation of calcium waves in Xenopus oocytes (Lechleiter *et al.*, 1991). The phenomenological similarity of these systems is reflected in their mathematical description, which is based on the general formalism of coupled reaction-diffusion equations (Tyson and Keener, 1988). The existence of additional chemotactic cell motion, following a non-diffusive mechanism, is an important particularity of the *Dictyostelium* system.

Martiel and Goldbeter (1987) proposed nonlinear kinetic rate laws describing oscillations and signal relay by *Dictyostelium* amoebae in well-stirred cell suspensions. These were extended by Tyson *et al.* (1989) to a reaction-diffusion model which is able to describe spatial pattern formation and implies the simplification of resting cells. In the real process amoebae are moving periodically and their motion interacts with the propagation of the chemical wave in a way which is not yet understood systematically (Alcantara and Monk, 1974). However, chemotaxis forces *Dictyostelium* cells to a movement in the direction of the strongest increase of cAMP-concentration (Fischer *et al.*, 1989). In an earlier study (Steinbock *et al.*, 1991) we found that the cell velocity in the periphery of

* Current address: West Virginia University, Department of Chemistry, Morgantown, WV 26506-6045, U.S.A.

Reprint requests to Dr. S. C. Müller.
Telefax: 49-231-1206389.

0939–5075/95/0300–0275 $ 06.00

wave patterns varies between nearly zero and 20–30 μm/min. The direction of the velocities of amoebae and chemical wave propagation are antiparallel; their magnitudes have a ratio of approximately 1:10. Probably only those spatial cAMP-gradients cause a chemotactic cell response that coincide with a local temporal increase in the cAMP-concentration.

This paper analyzes the chemotactic cell motion in the central region of spiral waves and target patterns in quantitative detail by applying a mutual-correlation method for the analysis of velocity fields. The method yields characteristic properties of attracting domains, which constitute a fascinating phenomenon of excitation patterns.

Materials and Methods

(1) Experimental

The cells of *Dictyostelium discoideum*, axenic strain AX-2, were cultivated on nutrient medium and harvested at a density of 5×10^6 cells/ml, washed three times with buffer and spread uniformly on an agar surface (containing 2 mM caffeine) in a Petri dish at a density of approximately 4×10^5 cells/cm^2. The dishes were stored in the dark at 21 °C for 4–6 hours. After this time the cell motion was detected with an inverse microscope (Zeiss IM 35) under bright-field illumination. The central region of the self-organizing structures (i.e. the spiral core or the pacemaker of a target pattern) was found by visual inspection. With a video camera (Hamamatsu C2400) and a time lapse video recorder (SONY EVT-801 CE) quick-motion movies (factor 25) were taken. A personal computer with an image acquisition card (Data-Translation, DT-2851) and an expanded memory card allows to store sequential image data of arbitrary size, image position and sampling speed. All subsequent calculations were performed on a Convex-C201 computer.

(2) Velocity analysis

A specific space-resolved velocity analysis (Miike *et al.*, 1986; Hashimoto *et al.*, 1995), based on a mutual correlation method, turns out to be suitable for obtaining quantitative information about the cell motion. A moving cell, showing a characteristic contour (e.g. the cell boundary), causes temporal intensity changes at the traversed sites of recorded picture elements (pixels). If the contour is nearly constant in time, the intensity functions of neighboring pixels are shifted due to the cell motion by a retardation time τ_0. This time shift is calculated by mutual-correlation functions $M_{0^k}(\tau)$ between the temporal brightness change of a central pixel at position 0 ($I_0(t) - \overline{I_0}$) and that of its neighboring pixels at position k ($I_k(t) - \overline{I_k}$):

$$M_0^k(\tau) = \frac{1}{T}\int_{-T}^{T} (I_0(t) - \overline{I_0})\,(I_k(t+\tau) - \overline{I_k})\mathrm{d}t$$

($\overline{I_0}$, $\overline{I_k}$ denote the mean values of $I_0(t)$ and $I_k(t)$). For digitized time series the integral is reduced to summation terms. The fraction of the pixel distance and the retardation time τ_0, when $M_{0^k}(\tau)$ reaches its maximum, yields the velocity v_{0^k} in direction towards the neighboring pixel k. The maximum value of $M_{0^k}(\tau)$ is a measure for the probability that the cell was moving towards the site k. Due to necessary restrictions to be made, a considerable number of pixels is omitted in the calculations (Hashimoto *et al.*, 1995). Therefore, we commonly use spatial averages in appropriately selected areas. Spatial averages also suppress the component of stochastic cell motion, which is, as a charateristic property of amoebae, superposed on their chemotactic movement.

Results

An example of a spiral-shaped cell aggregation pattern as obtained in the traditional dark-field illumination is presented in Fig. 1. In our velocity analysis microscopic sections of the pattern (bright-field illumination) are selected and recorded in digital image sequences. Microscopic quick-motion movies of the spiral core region (0.39×0.32 mm^2) reveal a circulating cell movement. One large sector always shows a higher cell velocity than the remaining area. This sector circulates, but its sense of rotation is opposite to that of the individual amoebae.

Mutual correlation analysis allows a quantitative description of this phenomenon. Fig. 2A shows a velocity field determined in an 0.39×0.32 mm^2 area of the central region of a spiral. This area was digitized to an array of 512×512 pixels, each with

Fig. 1. Dark-field photography of a spiral wave in a two-dimensional layer of aggregating *Dictyostelium discoideum* cells. The pattern has a wave length of approximately 3 mm and a rotation period of 8 min.

256 possible grey levels. The velocity vectors were estimated from time series of 30 images corresponding to 120 s in the experiment. In Fig. 2A each vector is calculated by averaging the available information of the 51×51 surrounding pixels.

Thus, the noise level due to the individual erra
motion of single amoebae is efficiently reduc
The vectors in Fig. 2A form a vortex like structu
with a faster motion in the upper excited segme
Here, the highest velocity v_{max} = 14.9 μm/min
detected. The slowest cell motion v_{min} = 1.3 μ
min is found in the central part of the veloc
field. In this region the chemical stimulus on t
amoebae seems to be weaker than in the otl
parts of the wave pattern. The excited segme
moves around the centre with a period of appro
mately 8 min.

In Fig. 2B temporal changes of the velocities
shown along a vertical cut (y-coordinate) thro
the centre of the velocity field in Fig. 2A.
changes $\Delta v(y)$ are calculated by substracting
local velocities at two different times t_0, t_1 fr
each other, where $t_0 - t_1$ = 4 min is approximat
half of one spiral period. For small y (the up
part of Fig. 2A) the velocities decrease, but
large y they increase.

For a more detailed spatial analysis we cal
lated streamlines describing the most proba
tracks of the amoebae. The applied algorithm c
structs each streamline iteratively for arbitr
starting points, using only the angle of the vel
ties. We tested the reliability of the algorithm
applying it to gradient fields derived from sim

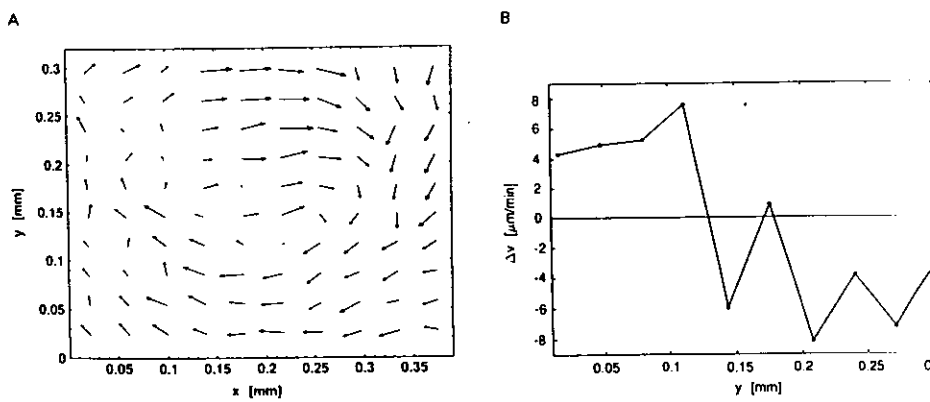

Fig. 2. (A) Velocity field of the chemotactic cell motion in the core region of a spiral wave pattern obtaine
mutual-correlation analysis. The motion of the *Dictyostelium* amoebae forms a vortex-like structure. In this ex
ment the agar contains 2 mM caffeine. Analyzed area: 0.39×0.32 mm^2. (B) Changes of cell velocity Δv over h
period of spiral rotation plotted against the y coordinate passing through the spiral core. The variable y corresp
to a vertical cut through the middle of the velocity field in Fig. 2A. The velocities are increasing for small
decreasing for large values of y. This behaviour is caused by an 180° rotation of the spiral tip.

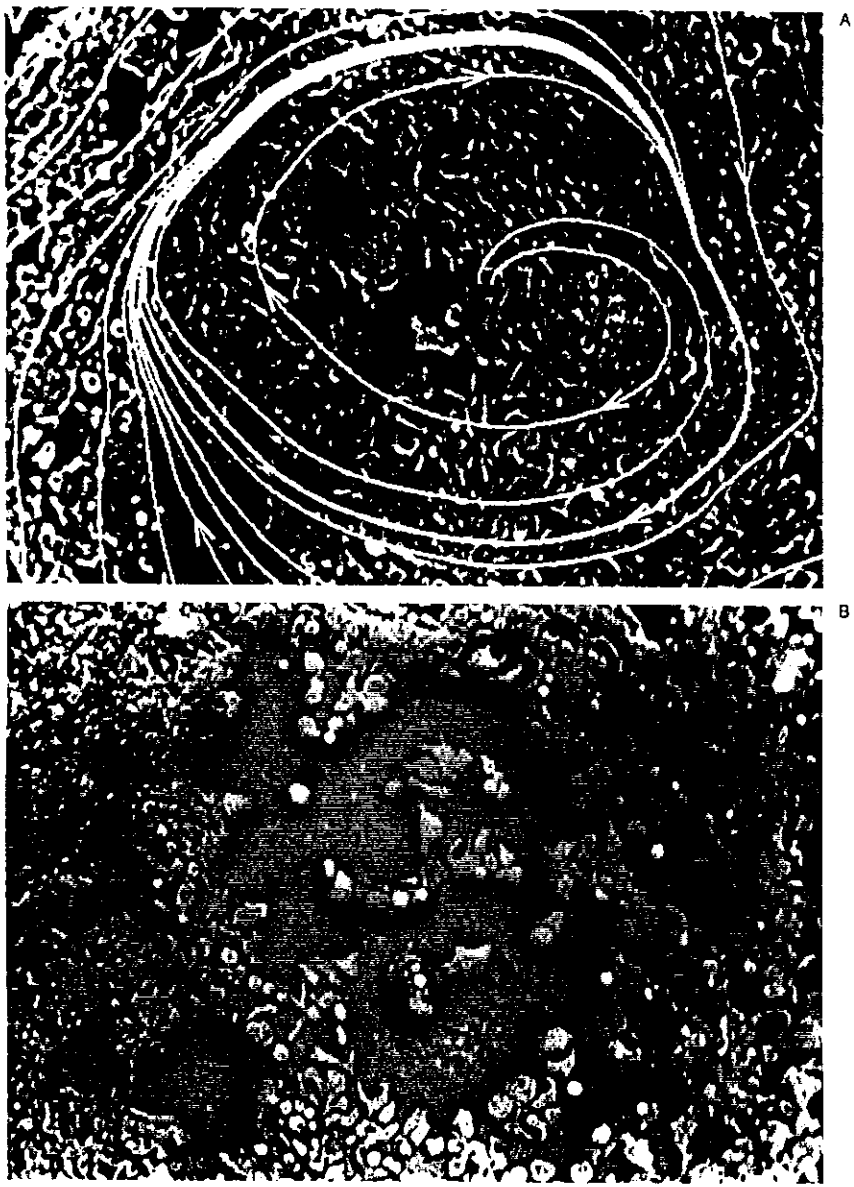

Fig. 3. (A) Streamlines calculated from the velocity field in Fig. 2A, describing the motion of the amoebae. The background shows one of the analyzed microscopic images of the core region. A closed curve seperates two different domains of cell movement. In the outer region, cells are aggregating in a circulating manner, in the inner region cells are led outwards on spiralling tracks. For this reason we call the closed curve of the streamline structure the spatial limit cycle of cell motion. (B) Microscopic image of the late stage of core region (2 mM caffeine). The image shows a 0.39×0.32 mm² section. A ring of high cell density encloses a region containing only a few amoebae. This hole is caused by cAMP-gradients in the spiral core leading cells slowly outwards.

mathematical formulae. The tests reveal good agreement between the reconstructed and theoretical curves. Fig. 3A gives a typical result of the analysis, based on the velocity field of Fig. 2. The streamlines are overlayed on a background showing one of the analyzed microscopic images of amoebae distribution.

It is remarkable that a closed streamline appears with the other trajectories nestling to this curve. The characteristic features of this movement are reminiscent of trajectories in phase space leading on a limit cycle. In a mathematically defined two-dimensional phase space representing solutions of a two-variable system of ordinary differential equations such a limit cycle is a closed path to which solutions are attracted asymptotically (Jordan and Smith, 1977). In our system, the area which is enclosed by the the spatial limit cycle has a size of 0.051 mm² and corresponds to the spiral core of the wave structure. A circle having the same area yields a core radius of approximately 0.13 mm. The cell movement along trajectories outside the closed curve possesses a dominating aggregative component. Inside the limit cycle the amoebae are led outside following spiral shaped tracks. This motion causes a decreasing cell density in the area inside the closed streamline. Fig. 3B shows a typical example of the resulting hole. The size of this hole covers the area of the observed limit cycles. Several spiral rotations later, we usually observed a decay of this arrangement into several new aggregation centres close to the hole. Dark-field images show that the pacemaker of the spiral wave in Fig. 1 vanishes and is replaced by three small target patterns, forming new individual centres.

By changing the caffeine concentration it is possible to control the core radius. Without added caffeine we find no detectable hole at all. With increasing caffeine concentration up to 5 mM the empty area is getting larger. One should notice that at this time the spiral shaped excitation wave circulates around a non-excitable region, without an effect on the basic spiral topology.

The central region of target patterns reveals significantly different chemotactic cell behaviour. In contrast to the vortex-like motion around spiral cores, we observed radial cell movement towards a singular point or very small domain. Fig. 4A shows a typical microscopic image (0.39×0.32

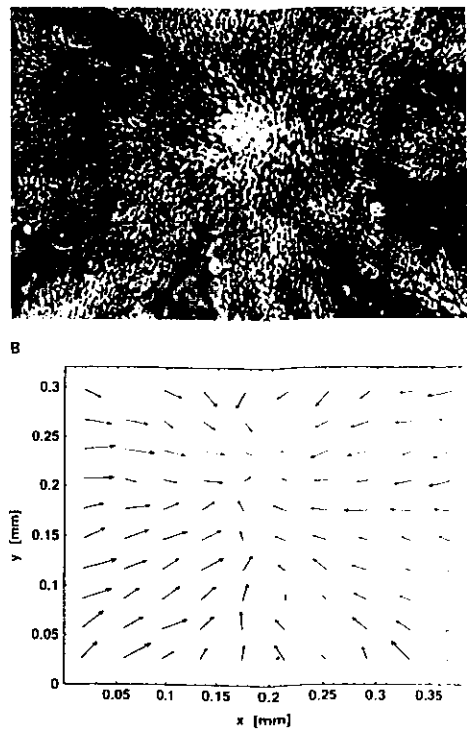

Fig. 4. (A) Microscopic image of the central region of target pattern (0.39×0.32 mm²; 2 mM caffeine). Quic motion pictures show that the amoebae move perio cally towards the central pacemaker. (B) Correspondi velocity field calculated from a 120 s sequence by mut correlation analysis. The pacemaker of a target patte controls cell aggregation like a star-shaped node attrac ing points in phase space.

mm²) of the centre of a target pattern. The corr lation analysis of this region, performed with t same parameters as for the spiral core region, given in the velocity-vector field of Fig. 4B. T velocities vary periodically, but reveal no signif cant angular dependence. Following the analo between attractors in the phase plane and the ch motactic cell behaviour, we denote this kind radial motion as spatial (star-shaped) nod Furthermore, the central part of target patter shows no formation of a disk with low cell densit

the number of cells increases continuously and the initially two-dimensional cell layer is slowly transformed to a three-dimensional mound.

Discussion and Conclusion

Our experimental results give quantitative information on the structure and dynamics of chemotaxis in the central region of spiral waves and target patterns. The analysis of pattern formation by measuring chemotactic cell response is a powerful tool, which reveals details that cannot be obtained with the common dark-field method. Furthermore, the complex chemotactic movement itself is a novel example documenting how structure formation occurs in nature.

The finding of a spatial limit cycle as the central attractor in spiral waves corresponds to the existence of a core in the central region of this aggregation process. The spiral tip spinning around this core leads to specific concentration gradients of cAMP, forcing the amoebae to the observed behaviour. Earlier investigations of spiral cores in the BZ reaction (Müller *et al.*, 1985; Plesser *et al.*, 1990) support this explanation and demonstrate the fascinating similarity of these systems: inside the chemical core analogous concentration gradients are oriented outwards. They change their direction continuously with increasing distance from the centre. Finally, in the periphery of spirals these gradients point exactly towards the core centre.

The formation of a central region of low cell density coincides with the emergence of a weakly or non-excitable disk. This process depends strongly on the caffeine concentration of the medium, which is an important parameter controlling the excitability of the system (Siegert and Weijer, 1989). Caffeine is known to inhibit the activation of the adenylate cyclase, while it has little effect on the cGMP formation which is associated with chemotaxis (Brenner and Thoms, 1984). Experiments in a light-sensitive version of the BZ reaction (Steinbock and Müller, 1992) have demonstrated an interesting analogy to the self-organized spiral cores of the slime mold system. Chemical spiral waves can rotate around laser-induced unexcitable spots ("artificial cores") that correspond to the central region of low cell density observed in the *Dictyostelium* system. The size of the laser spot changes the rotation period of the spiral, which is a characteristic constant value in homogeneous media. This correlation could explain the temporal evolution of the rotation frequency of spirals during the first two hours of *Dictyostelium* aggregation. Without caffeine Siegert and Weijer (1989) observed a nearly constant period (no holes). In the presence of caffeine (2 and 5 mM), however, they found the period to increase, because the diameter of the central hole influences the rotation period of the pattern just like in the BZ reaction.

In the central part of target patterns the chemotactic cell motion is controlled by a different spatial attractor (star-shaped node). In spite of the difference between spirals and target patterns the behaviour of amoebae in the periphery of these structures is the same. In conclusion, both types of attracting pacemakers guarantee an effective accumulation of cells, which is necessary for the formation of fruiting bodies.

It will be interesting to see, whether further numerical models, which include chemotactic transport, are able to simulate the described behaviour and elucidate the still open question of interaction between cell motion and wave propagation.

Alcantara F. and Monk M. (1974), Signal propagation during aggregation in the slime mould *Dictyostelium discoideum*. J. Gen. Microbiol. **85**, 321–334.
Brenner M. and Thoms S. D. (1984), Caffeine blocks activation of cyclic AMP synthesis in *Dictyostelium discoideum*. Developmental Biol. **101**, 136–146.
Fischer P. R., Merkl R. and Gerisch G. (1989), Quantitative analysis of cell motility and chemotaxis in *Dictyostelium discoideum* by using an image processing system and a novel chemotaxis chamber providing stationary chemical gradients. J. Cell Biol. **108**, 973–984.
Foerster P., Müller S. C. and Hess B. (1990), Curvature and spiral geometry in aggregation patterns of *Dictyostelium discoideum*. Development **109**, 11–16.
Hashimoto H., Miike H., Koga K. and Müller S. C. (1995), Two-dimensional velocimetry by spatiotemporal correlation analysis, submitted to Phys. Fluids.
Jakubith S., Rotermund H. H., Engel W., von Oertzen A. and Ertl G. (1990), Spatiotemporal concentration patterns in a surface reaction: propagating and standing waves, rotating spirals and turbulence. Phys. Rev. Lett. **65**, 3013–3016.
Jordan W. D. and Smith P. (1977), Nonlinear Ordinary Differential Equations. Oxford University Press, Oxford.
Lechleiter J., Girard S., Peralta E. and Clapham D. (1991), Spiral calcium wave propagation and annihilation in *Xenopus oocytes*. Science **252**, 123–126.
Loomis W. F. (1982), Development of *Dictyostelium*. Academic Press, San Diego.
Martiel J.-L. and Goldbeter A. (1987), A model based on receptor desensitization for cyclic AMP signalling in *Dictyostelium* cells. Biophys. J. **52**, 807–828.
Miike H., Kurihara Y., Hashimoto H. and Koga K (1986), Velocity field measurements by pixel-based temporal mutual-correlation analysis of dynamic image. Trans IEICE Japan **E69**, 877–882.
Müller S. C., Plesser T., and Hess B. (1985), The structure of the core of the spiral wave in the Belousov Zhabotinskii reaction. Science **230**, 661–663.
Plesser T., Müller S. C. and Hess B. (1990), Spiral wave dynamics as a function of proton concentration in the ferroin-catalyzed Belousov-Zhabotinskii reaction. Phys. Chem. **94**, 7501–7507.
Siegert F. and Weijer C. J. (1989), Digital image processing of optical density wave propagation in *Dictyostelium discoideum* and analysis of the effects of caffein and ammonia. J. Cell Sci. **93**, 325–335.
Steinbock O., Hashimoto H. and Müller S. C. (1991 Quantitative analysis of periodic chemotaxis in aggregation patterns of *Dictyostelium discoideum*. Physic **49D**, 233–239.
Steinbock O. and Müller S. C. (1992), Chemical spiral rotation is controlled by light-induced artificial core Physica **188A**, 61–67.
Tomchik K. J. and Devreotes P. N. (1981), Adenosin 3',5'-monophosphate waves in *Dictyostelium discoideum:* a demonstration by isotope dilution-fluorography. Science **212**, 443–446.
Tyson J. J. and Keener J. P. (1988), Singular perturbation theory of travelling waves in excitable media. Physic **32D**, 327–361.
Tyson J. J. and Murray J. D. (1989), Cyclic AMP wave during aggregation of *Dictyostelium amoebae*. Development **106**, 421–426.
Winfree A. T. (1972), Spiral waves of chemical activit Science **175**, 634–636.

Proc. Natl. Acad. Sci. USA
Vol. 90, pp. 7332–7335, August 1993
Biophysics

Three-dimensional waves of excitation during *Dictyostelium* morphogenesis

(chemotaxis/numerical simulations/self-organization/reaction–diffusion coupling)

OLIVER STEINBOCK*, FLORIAN SIEGERT†, STEFAN C. MÜLLER*, AND CORNELIS J. WEIJER†

*Max-Planck-Institut für molekulare Physiologie, Rheinlanddamm 201, D-4600 Dortmund 1, Federal Republic of Germany; and †Zoologisches Institut, Universität München, Luisenstrasse 14, D-8000 München 2, Federal Republic of Germany

Communicated by Howard C. Berg, April 1, 1993 (received for review January 4, 1993)

ABSTRACT **Cells in *Dictyostelium* slugs follow well-defined patterns of motion. We found that the chemotactic cell response is controlled by a scroll wave of messenger concentration in the highly excitable prestalk zone of the slug that decays in the less-excitable prespore region into planar wave fronts. This phenomenon is investigated by numerical solutions of partial differential equations that couple local nonlinear kinetics and diffusive transport of the chemotactic signal. In the interface of both regions a complex twisted scroll wave is formed that reduces the wave frequency in the prespore zone. The spatio-temporal dynamics of waves and filaments are followed over 33 periods of rotation. These results yield an explanation of collective self-organized cell motion in a multicellular organism.**

Spatio-temporal self-organization is a general phenomenon occurring in excitable media (1, 2). Propagating waves of excitation are observed in physical, chemical, and biological systems, as diverse as the CO oxidation on platinum (3), the Belousov–Zhabotinsky (BZ) reaction (4, 5), *Xenopus* oocytes (6), cardiac muscle (7), and the slime mold *Dictyostelium discoideum* (8, 9). In two dimensions, these systems show a variety of wave structures including concentric rings and spiral waves.

For wave patterns occurring during *Dictyostelium* aggregation, the underlying biochemical and cellular reactions are well investigated (10). The aggregation of single cells to form multicellular structures is directed by periodic signals of cAMP and chemotaxis. Cells in the aggregation center periodically produce the chemoattractant cAMP. The cAMP is secreted into the extracellular medium, where it diffuses away. Neighboring cells detect cAMP via cell surface receptors. The stimulated cells then produce huge amounts of cAMP, which they in turn secrete. This feedback process results in a wave-like propagation of the cAMP signal from cell to cell and from the aggregation center outward (10). Binding of cAMP to the receptor induces a phosphorylation of the receptor that leads to desensitization and the shut down of cAMP production. Extracellular phosphodiesterase degrades cAMP, which allows the system to recover. Immediately after stimulation the cells are refractory to further stimulation. This property ensures unidirectional outward propagation of the signal. Stimulated cells move chemotactically in the direction of increasing cAMP concentrations, thus producing periodic waves of inward-directed chemotactic movement. These waves are detected as optical density waves under dark-field illumination (9, 10).

Nonlinear differential equations coupling local reaction kinetics with diffusive transport can reproduce experimental observations on the BZ reaction and *Dictyostelium* aggregation qualitatively and quantitatively (11–14). Complex modes of wave propagation have been observed in three-dimensional reaction–diffusion systems (15)—e.g., scroll waves that emerge from a straight axis (filament). An untwisted scroll wave exhibits identical Archimedian spirals for each two-dimensional cut perpendicular to the filament. Such wave patterns have been studied in the BZ reaction (16, 17) and can undergo complicated changes in geometry as they travel along a gradient of excitability. For example, a scroll wave decomposes to a twisted scroll wave and then into planar waves when it propagates into a medium of lower excitability (18).

Recently, we have obtained (19) evidence that three-dimensional scroll waves organize the motion of cells in *Dictyostelium* slugs. The slug is a migratory stage during the developmental cycle of *Dictyostelium*, in which the behavior of 10^5 individual cells is coordinated to that of a single organism (Fig. 1). The direction of cell motion is controlled by propagating waves of cAMP concentration. Cell motion occurs in a direction opposite to the direction of wave propagation (10, 20). The anterior part of the slug (20% of all amebae) consists of prestalk cells, which ultimately build the stalk of the fruiting body. The remainder is formed by prespore cells that differentiate to spores in the fruiting body.

Model and Numerical Approach

Analysis of cell motion in slugs revealed that amebae in the prespore zone move straight forward in the direction of slug migration, whereas cells in the prestalk zone move perpendicular to the direction of slug migration, that is they rotate around the slug axis. This analysis suggested that the chemotactic signal spreads as a scroll wave in the front of the slug and converts into planar waves in the rear part. We proposed (19) that this complex mode of wave propagation was caused by a change in excitability along the long axis of the slug, based on the finding that during aggregation the cells that will become prestalk show high-frequency oscillations in optical density when isolated, whereas cells that will become prespore show slow oscillations (21).

To investigate whether an excitable system exhibits such behavior in three dimensions, we performed computer simulations. Martiel and Goldbeter (22) have developed a model that describes the process of receptor-mediated cAMP production and desensitization based on receptor phosphorylation. The three variables in this model take into account the extracellular cAMP concentration, the intracellular cAMP concentration, and the fraction of activated receptors. By assuming realistic values for rates of receptor phosphorylation and cAMP synthesis and degradation, this model could produce sustained cAMP oscillations. When coupled with diffusion, spiral wave propagation was observed. This model was reduced to a two-variable model that essentially shows

The publication costs of this article were defrayed in part by page charge payment. This article must therefore be hereby marked "*advertisement*" in accordance with 18 U.S.C. §1734 solely to indicate this fact.

Abbreviation: BZ, Belousov–Zhabotinsky.

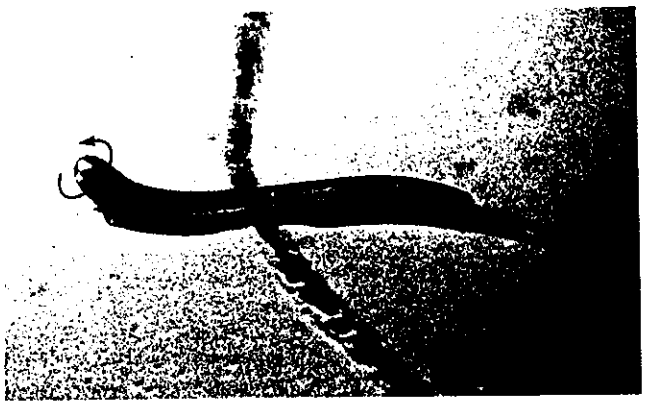

FIG. 1. *D. discoideum* slug. The tip (left side) rises up in the air. The prestalk zone (anterior 20%) is stained with the vital dye neutral red and is slightly darker in the photograph. The direction of cell motion is indicated by the arrows. In the prestalk zone, the cells rotate around the tip, whereas in the prespore zone (posterior 80%), the cells move forward in direction of the tip (18). The slug leaves a slime trail behind that is secreted by all cells. In the photograph, the slug crosses a slime trail left behind by another slug.

the same features such as oscillations and spiral wave propagation (22, 23).

Our main interest is to study wave propagation in an inhomogeneous excitable medium in three dimensions. This requires the numerical solution of sets of nonlinear partial differential equations. We have chosen the two-variable Barkley model (24) that produces the same features as the three-variable Martiel–Goldbeter model but is optimized for efficient numerical solution:

$$\frac{\partial u}{\partial t} = D_u \Delta u + \frac{1}{\varepsilon} u(1-u)\left(u - \frac{v+b}{a}\right)$$

and

$$\frac{\partial v}{\partial t} = u - v,$$

where diffusion coefficient $D_u = 1.0$ and parameters $a = 0.4$, $\varepsilon = 1/150$, and b specify the excitability of the system. The propagator u and the controller species v are functions of time and the three spatial coordinates. The variable u obeys nonlinear reaction kinetics and qualitatively models the extracellular cAMP concentration, and v represents the fraction of the cAMP receptors in the active state. The shape of the *Dictyostelium* slug is approximated by a cylinder (length, 100 grid points; diameter of cross section, 34 grid points). The total number of grid points (90,800) is of the same magnitude as the number of amebae in a typical slug. The cylinder is embedded in a rectangular box, surrounded by grid points obeying unexcitable kinetics ($b = 0.3$). Consequently, a flux of u through the cylindric boundary takes place, simulating loss to the slime sheath covering the slug. The difference in excitability between the prestalk and prespore region is modeled by a step function of parameter b along the symmetry axis of the cylinder ($b_{pst} = 0.01$ and $b_{psp} = 0.023$).

The diameter L of the circular cross section and the time step Δt are chosen to be $L = 21.25$ and $\Delta t = 0.041$. The Laplacian term is estimated from the six closest neighboring points. All calculations were performed on a Sun-IPX workstation and visualized by Sunvision software.

Results

The initial condition is an untwisted scroll wave along the long axis of the slug having constant excitability ($b_{pst} = b_{psp} = 0.01$) that stably rotates in the homogeneous system. After some time ($t = 880$ iterations), a change in excitability along the slug's long axis, as described above, is introduced. The scroll wave undergoes a complex transformation into a new pattern, as shown in the image sequence in Fig. 2. While the wave rotation in the region of high excitability (prestalk region) remains stable during the entire calculation, the scroll wave in the region of low excitability (prespore region) increases its wavelength and rotation period. Subsequently, the whole structure becomes twisted in middle segments of the cylinder (Fig. 2*A*). The process of twisting and the higher frequency in the prestalk region cause a dramatic change of

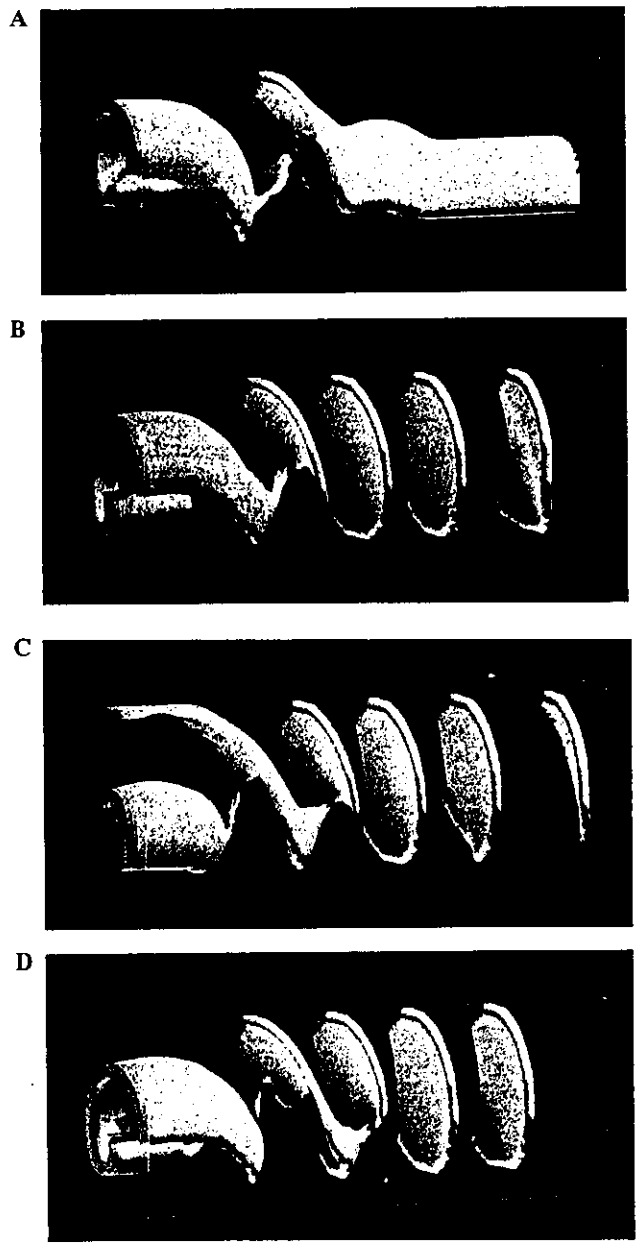

FIG. 2. Three-dimensional representation of the variable v ($v < 0.27$ transparent). The cylindrical excitable medium is separated in a high-excitable (left 20%, prestalk zone) region and a low-excitable (right 80%, prespore zone) region. The step of excitability destroys the initial scroll wave (*A*) and transforms it into planar waves in the right part (*B–D*). The depicted combination of wave structures explains the coordination of chemotactic cell motion in *Dictyostelium* slugs (see Fig. 1). Relative times of the pictures: t_a, 2600 iterations; t_b, 7800; t_c, 8000; t_d, 8200. The excitability step is initiated after 880 iterations.

the pattern in the less-excitable prespore zone: Planar wave fronts appear that are oriented perpendicular to the long axis of the cylinder (Fig. 2 *B–D*). Detailed analyses show that the shape of these wave fronts is slightly convex, thus focusing cell motion and stabilizing the slug geometry. This spatial arrangement is then stable over more than 30 periods of scroll wave rotation. The interface between the region of scroll wave rotation and planar wave propagation displays more complex dynamics and alternating phases of weak and strong twisting.

Fig. 3 showing the filament of wave rotation helps to elucidate the dynamics of this region. While the filament in the prestalk zone is generally oriented along the long axis of the slug, it becomes helical at the interface and bends away from the axis before ending at the cylinder boundary. Movies of the filament evolution reveal irregular changes in location and shape, but most of the time it stays attached to the boundary.

The space–time portrait in Fig. 4 describes dynamic features of the simulation. It consists of 324 two-dimensional spatial cuts (40,000 grid points) of the cylinder. The time between each spatial cut is 50 iterations. The left side of the space–time box (the prestalk zone) shows unperturbed wave propagation, and the right side shows the less-excitable prespore region and illustrates the decay of the initial scroll wave to planar fronts. The top of the box reveals an important consequence of the alternating wave form in the interface. Some of the emitted waves disappear at the right side of the interface or fuse with following ones. This mechanism reduces the number of waves in the prespore region and leads to frequencies that can be supported by this less-excitable medium.

The described behavior occurs in a range of values of b in the prespore region (e.g., $b_{psp} = 0.0245, 0.026$). For values of b_{psp} smaller than 0.021, the whole prespore region shows twisted scroll waves with large wavelengths. In these calculations, the helical filament terminates at the rear end of the cylinder.

Conclusions

Our calculations demonstrate that the observed pattern of chemotactic cell motion in *Dictyostelium* slugs (19) can be readily explained by scroll waves of a chemotactic signal in the prestalk zone that decay into planar wave fronts in the prespore zone. This change in the pattern of wave propagation is caused by a change in excitability along the long axis of the slug. The data are well fitted by the assumption that the change in excitability coincides with the prestalk–prespore boundary. The simulations have, furthermore, shown that the filament of the scroll wave in the prestalk zone is a stable structure, a region of steady and low concentration of the excitation variable, conditions that most likely direct stalk formation by controlling expression of stalk-specific genes (19).

These simulations explain the coordination of collective motion in a multicellular organism. They show that waves of excitation play a crucial role not only during aggregation but also during later three-dimensional morphogenesis in *Dictyostelium*. Our results also provide a simple explanation for complex modes of wave propagation in inhomogeneous excitable systems such as specific three-dimensional BZ media (18) or cardiac muscle (7).

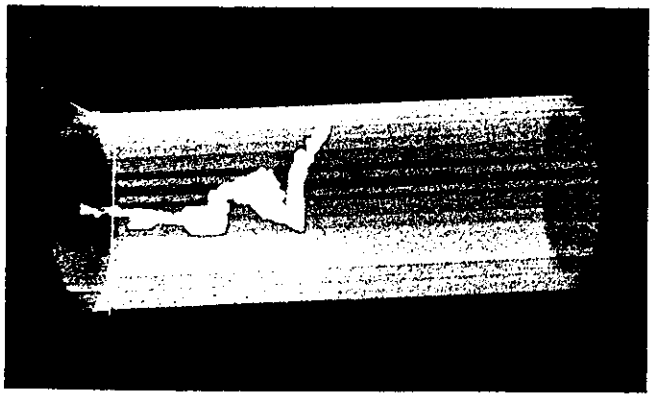

FIG. 3. Filament of wave rotation and boundary between the cylindrical excitable region and the unexcitable surroundings. The filament describes the set of spatial points having a low maximum value of u and v during one rotation of the scroll wave (420 iterations). Calculations are after 26 periods of scroll wave rotation.

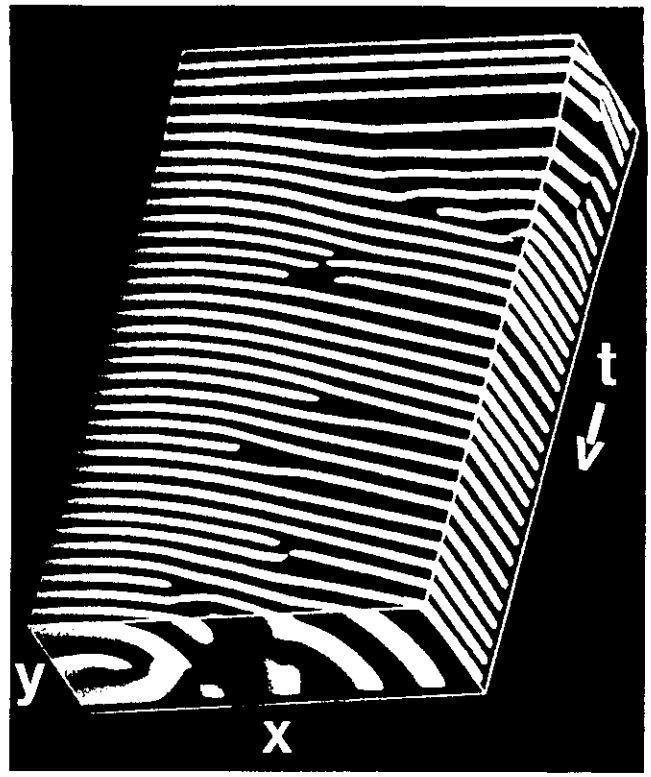

FIG. 4. Space–time portrait (x, y, and t) constructed from two-dimensional spatial cuts along the symmetry axis of the cylinder. The front side of the box shows the last (t = 16,200 iterations) spatial cut. The high-excitable prestalk zone is located on its left side, depicting a cut of the scroll wave that decays to perpendicular wave fronts. The top view illustrates the temporal transformation of scroll wave fronts (horizontal stripes) into waves propagating into the right prespore zone (tilted stripes).

1. Swinney, H. L. & Krinsky, V. I., eds. (1991) *Waves and Patterns in Chemical and Biological Media, Physica D* (North-Holland, Amsterdam), Vol. 49.
2. Markus, M., Müller, S. C. & Nicolis, G., eds. (1988) *From Chemical to Biological Organization* (Springer, Berlin).
3. Jakubith, S., Rotermund, H. H., Engel, W., von Oertzen, A. & Ertl, G. (1990) *Phys. Rev. Lett.* **65**, 3013–3016.
4. Zaikin, A. N. & Zhabotinsky, A. M. (1970) *Nature (London)* **225**, 535–537.
5. Field, R. J. & Burger, M., eds. (1985) *Oscillations and Travelling Waves in Chemical Systems* (Wiley, New York).
6. Lechleiter, J., Girard, S., Peralta, E. & Clapham, D. (1991) *Science* **252**, 123–126.
7. Davidenko, J. M., Pertsov, A. V., Salomonsz, R., Baxter, W. & Jalife, J. (1992) *Nature (London)* **355**, 349–351.
8. Tomchik, K. J. & Devreotes, P. N. (1981) *Science* **212**, 443–446.
9. Siegert, F. & Weijer, C. J. (1989) *J. Cell Sci.* **93**, 325–335.
10. Devreotes, P. N. (1989) *Science* **245**, 1054–1058.

11. Keener, J. P. & Tyson, J. J. (1986) *Physica D* **21**, 307–324.
12. Tyson, J. J. & Murray, J. D. (1989) *Development* **106**, 421–426.
13. Foerster, P., Müller, S. C. & Hess, B. (1990) *Development* **109**, 11–16.
14. Foerster, P., Müller, S. C. & Hess, B. (1988) *Science* **241**, 685–687.
15. Winfree, A. T. (1990) *SIAM* **32**, 1–53.
16. Welsh, B. J., Gamatam, J. & Burgess, A. E. (1983) *Nature (London)* **304**, 611–614.
17. Tzalmona, A., Armstrong, R. L., Menzinger, M., Cross, A. & Lemaire, C. (1990) *Chem. Phys. Lett.* **174**, 199–202.
18. Yamaguchi, T. & Müller, S. C. (1991) *Physica D* **49**, 40–46.
19. Siegert, F. & Weijer, C. J. (1992) *Proc. Natl. Acad. Sci. USA* **89**, 6433–6437.
20. Steinbock, O., Hashimoto, H. & Müller, S. C. (1991) *Physica D* **49**, 233–239.
21. Weijer, C. J., MacDonald, S. A. & Durston, A. J. (1984) *Differentiation* **28**, 13–23.
22. Martiel, J.-L. & Goldbeter, A. (1987) *Biophys. J.* **52**, 807–828.
23. Tyson, J. J., Alexander, K. A., Manoranjan, V. S. & Murray, J. D. (1989) *Physica D* **34**, 193–207.
24. Barkley, D. (1991) *Physica D* **49**, 61–70.

Communication

Vol. 271, No. 2, Issue of January 12, pp. 627–630, 1996

Traveling NADH and Proton Waves during Oscillatory Glycolysis *in Vitro**

(Received for publication, October 10, 1995, and in revised form, November 9, 1995)

Thomas Mair‡ and Stefan C. Müller

From the Max-Planck-Institut für molekulare Physiologie, Rheinlanddamm 201, 44139 Dortmund, Germany

Propagation and mutual annihilation of circular and spiral NADH and proton waves were detected by spatially resolved spectrophotometry and fluorescent proton indicators in a biological *in vitro* system: an organelle-free yeast extract. Spontaneous wave generation during glycolytic sugar degradation is established after an induction period of about 1 h. Controlled wave initiation could be performed by local injection of the strong activator of phosphofructokinase, fructose 2,6-bisphosphate. A crucial role for wave initiation and control of pattern dynamics is attributed to the key enzyme of glycolysis, the allosterically regulated phosphofructokinase. An overall increase in the concentration of its positive effector AMP leads to the formation of rotating spirals. The dynamics of the observed wave patterns resemble that of self-organized calcium waves as recently found in frog eggs and heart cells.

Living cells represent thermodynamically open systems, characterized by a nonequilibrium state. Their metabolism is often regulated by the action of enzymes with nonlinear, oscillatory reaction kinetics. A well known example is periodic oscillations in the degradation of sugar via glycolysis in resting yeast or heart cells (1–3). Investigations of spatially extended chemical nonequilibrium systems have demonstrated that nonlinear reaction kinetics, coupled with a transport process such as molecular diffusion, lead to the formation of self-organized waves (4, 5). Since similar thermodynamic principles apply for biological pathways, it has been suggested that wave patterns should occur in living cells, too (6, 7). First evidence for intracellular waves came from measurements of the spatial distribution of calcium in inositol 1,4,5-trisphosphate-activated frog eggs and in heart cells (8, 9). The observed calcium patterns and wave dynamics share great similarity with the patterns generated in chemical systems, suggesting that principles of self-organization hold for both systems.

For a detailed examination of the underlying mechanisms of intracellular self-organization one needs an *in vitro* system for experimental manipulations that are hard to perform with living cells. For this purpose, we chose glycolytic degradation of sugars in a yeast extract as a model system for such investigations. Under appropriate metabolic conditions glycolysis is characterized by oscillatory reaction kinetics (10–12) and fulfills all requirements for the generation of excitation waves: a nonequilibrium state and nonlinear reaction kinetics. Glycolytic degradation of sugars has been the subject of intense experimental and theoretical work regarding its metabolic control points and its nonlinear dynamic properties (13–17). Although several attempts were made to detect spatiotemporal patterns associated with oscillatory glycolysis in a yeast extract (18, 19), traveling excitation waves have yet not been shown. The aim of the present work is to demonstrate the generation of excitation waves during oscillatory glycolysis and to give first insights into the control of the pattern formation process.

MATERIALS AND METHODS

Cell extract was prepared from aerobically grown yeast according to Ref. 1 except that the yeast cells were ground with glass beads in a Braun-Melsungen homogenizer and the phosphate buffer was replaced by 25 mM MOPS,[1] 50 mM KCl, pH 6.5. For the detection of NADH waves 90 μl of yeast extract (40 mg of protein/ml) was mixed with 12.5 μl of 1 M trehalose, 6.3 μl of 1 M phosphate, pH 6.5, 4.3 μl of 3 M KCl, and 11.3 μl of twice distilled water. This mixture was then pipetted into a totally sealed reaction chamber and placed in the light beam of a two-dimensional spectrophotometer (λ= 340 nm; *cf.* Ref. 20). Spatially resolved absorption was monitored with a UV-sensitive camera (Hamamatsu C 1000), and the resulting movie was stored on a video recorder (SONY time lapse recorder EVT 801 CE). Image processing was performed with the Khoros program (version 1.05) on a SUN SPARC station. Proton waves were monitored with the fluorescent proton indicator fluorescein, using an inverted microscope (Zeiss IM 35). The excitation wavelength was set to 490 nm, and emission was recorded above 520 nm. For analysis of NADH concentration changes the gray levels of a selected image area of 40 × 40 pixels out of 512 × 512 pixels were summed up, and the arithmetic mean was plotted as a function of time.

RESULTS

In free open solution layers evaporative cooling easily leads to the generation of convective currents, which in turn can form stationary mosaic type patterns (21). Such structures can mask the appearance of excitation patterns. To avoid disturbances by convection we used a totally sealed reaction chamber for our experiments. During the measurement the yeast extract was not stirred in order to enable the development of spatial inhomogeneities in the probe. When mixed with its glycolytic substrates trehalose and phosphate, the yeast extract exhibits an initial phase of oscillatory concentration changes of NADH, which lasted for about 60 min (Fig. 1*e*). We call this phase the "induction period." No spatial inhomogeneities could be observed during this phase of glycolytic activity. The induction period is followed by a continuous increase in the average NADH concentration (corresponding to a decrease in transmitted light intensity). It is during this phase of NADH increase (at 60 min) that spontaneously generated circular NADH waves develop from the boundary with a frequency of 0.05 min^{-1} and start to propagate through the probe (*arrows* in Fig. 1*e*). Since there are multiple foci of wave generation, several waves move toward each other. The collision of NADH fronts results in their mutual annihilation (Fig. 1, *a* and *b*). The wave velocity amounts to about 5 μm/s and is constant throughout the passage of one wave, thus agreeing well with predictions from model calculations (6, 7). The velocity of the following waves gradually decreases for each subsequent one.

During glycolytic sugar degradation there is a production of

* The costs of publication of this article were defrayed in part by the payment of page charges. This article must therefore be hereby marked "*advertisement*" in accordance with 18 U.S.C. Section 1734 solely to indicate this fact.

‡ To whom correspondence should be addressed. Fax: 49-231-1206389. E-mail: thomas.mair@mpi-dortmund.mpg.de.

[1] The abbreviation used is: MOPS, 4-morpholinepropanesulfonic acid.

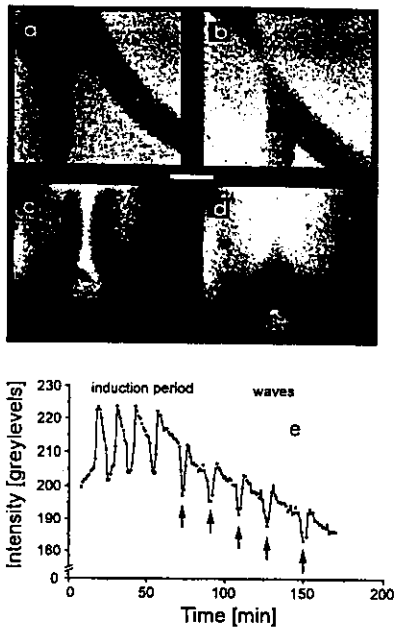

FIG. 1. **Propagation and annihilation of NADH and proton waves in a yeast extract.** Yeast extract was mixed with 100 mM trehalose, 50 mM phosphate, pH 6.5, and 100 mM KCl (final concentrations). NADH waves (*a* and *b*) were detected by spatially resolved spectrophotometry as described under "Materials and Methods." In a separate experiment, proton waves (*c* and *d*) were visualized with the fluorescent proton indicator fluorescein (100 μM) using an inverted microscope. *a–d* represent single snapshots of propagating waves. The time interval between images *a* and *b* is 384 s and between *c* and *d* is 240 s. Scale *bar* is 1 mm for *a* and *b* and 2 mm for *c* and *d*. Concentration changes of NADH during the experiment were monitored by gray level analysis (*e*). During the first 60 min, oscillations but no spatial inhomogeneities were observed (induction period). Thereafter, a state of spontaneous wave formation occurs. *Arrows* in *e* indicate the passage of NADH waves through the selected frame for gray level analysis.

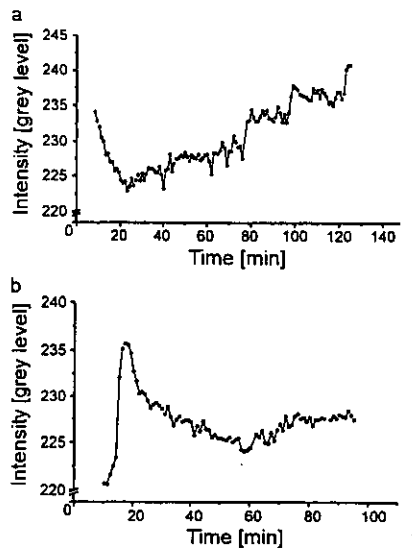

FIG. 2. **Suppression of oscillations in a yeast extract when EDTA is present or trehalose is replaced by glucose.** Experimental procedures and data analysis are the same as described for Fig. 1*e*. The composition of yeast extract is as in Fig. 1, except that 5 mM EDTA was added (*a*) or trehalose was replaced by 10 mM glucose (*b*).

protons by ATP hydrolysis, oscillating with a phase shift of about 30° with respect to the NADH oscillations (11). In addition, NADH itself is associated with a proton. Thus, it is probable that proton waves are generated in the system as well. In fact, when using the fluorescent proton indicator fluorescein, proton waves were detected (Fig. 1, *c* and *d*) with a shape and wave dynamics being similar to that of the NADH wave patterns (compare images *a* and *b* with *c* and *d* in Fig. 1).

Control experiments were performed to check whether the generation of waves is correlated to the oscillatory reaction of the glycolytic pathway. EDTA was added to the yeast extract to complex magnesium. In the absence of magnesium the glycolytic enzymes phosphofructokinase and pyruvate kinase are no longer active and glycolysis is stopped. Replacement of trehalose by glucose leads to an increased glycolytic flux through phosphofructokinase without oscillatory reaction (11). As shown in Fig. 2 in both experiments no oscillations occur and no NADH waves are generated.

It is now widely accepted that phosphofructokinase acts as the primary source of glycolytic oscillations *in vitro*. Due to a model of Sel'kov (17) autocatalysis is achieved by feedback control of phosphofructokinase by adenine nucleotides. Having this model in mind, we manipulated the adenine nucleotide pool by addition of AMP in order to influence phosphofructokinase regulation and thereby wave propagation dynamics.

We found that a stepwise increase of AMP addition from 0.25 to 1 mM did not lead to remarkable changes of the oscillatory frequency during the induction period nor of the wave velocity (Table I). However, shape and dynamics of the wave patterns alter markedly. In the investigated concentration range of AMP, wave fronts break up spontaneously and open wave ends curl up to form rotating spirals (Fig. 3, *a–d*). The motion of the spiral tip proceeds along a loop-shaped trajectory (Fig. 3*e*) resembling patterns of spiral trajectories known from the chemical Belousov-Zhabotinski reaction with reduced excitability (so-called meandering (22)). One loop was completed after about 25 min. Without added AMP spontaneous break up of circular fronts also occurs, but open wave ends fail to curl up.

Controlled wave initiation could be carried out with the very potent activator of phosphofructokinase, fructose 2,6-bisphosphate (*cf.* Ref. 23). After the induction period has passed, a local injection of 0.5 mM fructose 2,6-bisphosphate (estimated final overall concentration, 5–20 μM) leads to generation and propagation of NADH waves (Fig. 4). When injected in the back of a wave, fructose 2,6-bisphosphate did not initiate a new NADH wave. To exclude artifacts of solvents, water or 2 mM KOH (solvent for fructose 2,6-bisphosphate) was injected instead of fructose 2,6-bisphosphate. No NADH waves could be initiated in these control experiments.

DISCUSSION

The presented data give evidence that traveling excitation waves can be generated in a biological *in vitro* system. From chemical systems it is known that such waves are followed by a refractory zone, where inhibitor must be degraded before a new wave can pass through it (for review see Ref. 24). Besides their spontaneous formation (Fig. 1), NADH waves can be generated by injection of fructose 2,6-bisphosphate (Fig. 4), indicating the excitable character of the yeast extract. The failure to induce waves by injection of fructose 2,6-bisphosphate into the back of a NADH wave clearly demonstrates the existence of the refractory zone. This zone is responsible for the mutual annihilation of colliding waves as shown in Fig. 1. It has, besides the excitability of the system, an important influence in determining the formation of spiral-shaped waves from open wave ends. If the refractory zone is too large or the excitability too low, spirals do not develop (25). Thus, the formation of rotating spirals, which is the main effect of AMP addition, can result either from a reduction of the refractory zone or an increase of excitability.

Phosphofructokinase as the primary source of glycolytic oscillations plays an important role for control of wave dynamics. Its importance is pointed out by the results of wave initiation

TABLE I

Effect of AMP on spatiotemporal dynamics in glycolysis

Frequencies of oscillations (during induction period) and wave generation were determined by gray level analysis as shown in Fig. 1*e*. Wave velocity was measured by evaluation of the space coordinates of propagating planar waves on a TV screen. The results represent the mean (±S.D.) of 2–3 independent measurements.

	AMP addition (mM)				
	0	0.25	0.5	0.75	1
Frequency of autooscillations (min^{-1})	0.081 ± 0.009	0.077 ± 0.007	0.073 ± 0.009	0.070 ± 0.008	0.071 ± 0.009
Frequency of wave generation (min^{-1})	0.049 ± 0.006	0.046 ± 0.008	0.044 ± 0.008	0.041 ± 0.007	0.039 ± 0.007
Wave velocity ($\mu m\ s^{-1}$)	5.33 ± 1	5.17 ± 0.9	4.53 ± 0.8	4.81 ± 0.8	3.99 ± 0.3

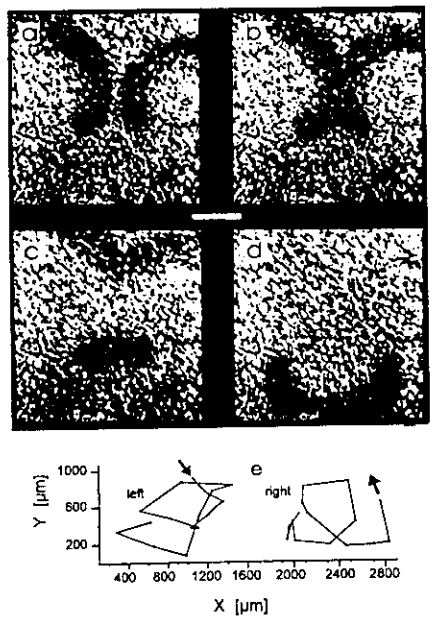

FIG. 3. **Spontaneously generated spiral-shaped NADH waves by an overall increase in AMP concentration.** Experimental procedures and composition of yeast extract are as described for Fig. 1, except that 0.25 mM AMP was added to the yeast extract concomitantly with trehalose, phosphate, and KCl. Spontaneous break up of wave fronts and subsequent spiral formation were observed after the induction period had passed (compare with Fig. 1). The time interval between images *a* and *b* is 90 s, between *b* and *c* is 105 s, and between *c* and *d* is 392 s. *Bar* corresponds to 1 mm. The trajectories of the left and right spiral tip are shown in *e*. *X* and *Y* are space coordinates. *Arrows* indicate direction of tip movement.

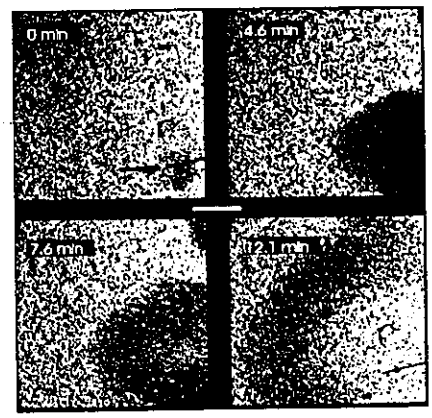

FIG. 4. **Initiation of NADH waves by locally applied fructose 2,6-bisphosphate.** Experimental procedures and composition of yeast extract are as described for Fig. 1. After the induction period, wave initiation was performed between the passage of two subsequent spontaneously formed waves at the initiation site. A glass capillary tip (diameter, ≈5 µm) filled with fructose 2,6-bisphosphate (0.5 mM dissolved in 1 mM KOH) was inserted into the probe, and the sugar phosphate was injected by air pressure (indicated by an *arrow*). Timing of images is indicated. Scale *bar* corresponds to 1 mm.

with fructose 2,6-bisphosphate. The effect of AMP is most probably also related to phosphofructokinase activity. Either it stimulates phosphofructokinase activity and thereby leads to an increased breakdown of the enzyme's inhibitor (and substrate) ATP or the overall increase of adenine nucleotides by AMP addition reduces the sensitivity of the enzyme to ATP. The autocatalytic reaction of phosphofructokinase is a necessary prerequisite for wave generation, as shown by the control experiments with EDTA or glucose (Fig. 2). In view of this finding, the meaning of allosteric regulation of phosphofructokinase for oscillatory glycolysis should be extended to the control of spatial patterns.

Circular and spiral calcium waves in frog eggs, as an another example for intracellular self-organization, exhibit similar patterns. Despite their similar wave dynamics, there are significant differences in the mechanisms of wave propagation. Whereas calcium waves propagate via a calcium-induced calcium release mechanism, requiring the existence of cellular calcium stores (8, 26), NADH and proton waves propagate by simple diffusion in an evenly distributed enzyme solution. Moreover, calcium waves develop without a pronounced time delay after the onset of the inositol trisphosphate signal transduction pathway, whereas glycolytic NADH and proton waves are generated after a prolonged induction period. We assume that accumulation of glycolytic intermediates and/or end products during the induction period is necessary for spontaneous NADH wave formation. It is likely that NADH and proton waves interact with organelles and thereby with calcium waves, either via electrochemical gradients and/or NADH oxidizing enzymes. Interactions between calcium signaling pathways and glycolysis have been already shown in rat pancreatic β-cells (27–29).

The occurrence of proton waves provides a way in which glycolysis-induced excitation patterns can interact with electric fields. Membrane potential changes, driven by oscillations of intracellular NADH, already could be observed in heart cells (30). Yet, it is not clear whether the glycolytic proton waves originate from the NADH-associated proton or whether they are produced in the upper glycolytic pathway. In order to clarify the origin of the proton waves in glycolysis, simultaneous measurements of both compounds, NADH and protons, are necessary.

It is remarkable that both oscillatory behavior and generation of excitation waves manifest a change in the cellular state. This might serve as an indication for their role in cellular information processing (31, 32). Since NADH and proton waves represent highly ordered structures of molecules that are involved in the cellular energy metabolism, they can act as spatially resolved signals of the energetic status of the cell.

Acknowledgments—We thank R. Goody, V. Zykov, A. Boiteux, and K. Matthiessen for support and valuable discussions. D. Stock and B.

Schmidt are acknowledged for help in computer programming and A. Warda for excellent technical assistance.

REFERENCES

1. Hess, B., and Boiteux, A. (1968) *Hoppe-Seyler's Z. Physiol. Chem.* **349,** 1567–1574
2. Betz, A., and Chance, B. (1965) *Arch. Biochem. Biophys.* **109,** 585–594
3. Chance, B., Williamson, J. R., Jamieson, D., and Schoener, B. (1965) *Biochem. Z.* **341,** 357–377
4. Zaikin, A. N., and Zhabotinsky, A. M. (1970) *Nature* **225,** 535–537
5. Winfree, A. T. (1972) *Science* **175,** 634–636
6. Goldbeter, A. (1973) *Proc. Natl. Acad. Sci. U. S. A.* **70,** 3255–3259
7. Marmillot, P., Hervagault, J.-F., and Welch, G. R. (1992) *Proc. Natl. Acad. Sci. U. S. A.* **89,** 12103–12107
8. Lechleiter, J. D., and Clapham, D. E. (1992) *Cell* **69,** 283–294
9. Lipp, P., and Niggli, E. (1993) *Biophys. J.* **65,** 2272–2276
10. Chance, B., Schoener, B., and Elsaesser, S. (1965) *J. Biol. Chem.* **240,** 3170–3181
11. Hess, B., Boiteux, A., and Krüger, J. (1968) *Adv. Enzyme Regul.* **7,** 149–167
12. Das, J., and Busse, H.-G. (1991) *Biophys. J.* **60,** 369–379
13. Boiteux, A., Goldbeter, A., and Hess, B. (1975) *Proc. Natl. Acad. Sci. U. S. A.* **72,** 3829–3833
14. Tornheim, K., Andres, V., and Schultz, V. (1991) *J. Biol. Chem.* **266,** 15675–15678
15. Tremonia, Y., and Ross, J. (1981) *Proc. Natl. Acad. Sci. U. S. A.* **78,** 2952–2956
16. Aon, M. A., Cortassa, S., Westerhoff, H. V., Berden, J. A., Van Spronsen, E., and Van Dam, K. (1991) *J. Cell Sci.* **99,** 325–334
17. Sel'kov, E. E. (1968) *Eur. J. Biochem.* **4,** 79–86
18. Boiteux, A., and Hess, B. (1978) in *Frontiers of Biological Energetics* (Dutton, P. L., Leigh, J., and Scarpa, A., eds) Vol. I, pp. 789–797, Academic Press, New York
19. Jacobsen, H., Busse, H. G., and Havesteen, B. H. (1982) *J. Biol. Chem.* **257,** 4001–4006
20. Müller, S. C., Plesser, T., and Hess, B. (1985) *Anal. Biochem.* **146,** 125–133
21. Müller, S. C., Plesser, T., and Hess, B. (1985) *Ber. Bunsen-Ges. Phys. Chem.* **89,** 654–658
22. Nagy-Ungvarai, Z., Ungvarai, J., and Müller, S. C. (1993) *Chaos* **3,** 15–19
23. Hers, H. G. (1984) *Biochem. Soc. Trans.* **12,** 729–735
24. Tyson, J. J., and Keener, J. P. (1988) *Physica D* **32,** 327–361
25. Mikhailov, A. S., and Zykov, V. S. (1991) *Physica D* **52,** 379–397
26. Berridge, M. J. (1990) *J. Biol. Chem.* **265,** 9583–9586
27. Corkey, B. E., Deeney, J. T., Glennon, M. C., Matschinsky, F. M., and Prentki, M. (1988) *J. Biol. Chem.* **263,** 4247–4253
28. Corkey, B. E., Tornheim, K., Deeney, J. T., Glennon, M. C., Parker, J. C., Matschinsky, F. M., Ruderman, N. B., and Prentki, M. (1988) *J. Biol. Chem.* **263,** 4254–4258
29. Dukes, I. A., McIntyre, M. S., Mertz, R. J., Philipson, L. H., Roe, M. W., Spencer, B., and Worley, J. F., III (1994) *J. Biol. Chem.* **269,** 10979–10982
30. O'Rourke, B., Ramza, B. M., and Marban, E. (1994) *Science* **265,** 962–966
31. Berridge, M. J., Cobbold, P. H., and Cuthbertson, K. S. R. (1988) *Philos. Trans. R. Soc. Lond. B Biol. Sci.* **320,** 325–343
32. Goldbeter, A. (ed.) (1989) *Cell to Cell Signaling: From Experiments to Theoretical Models*, Academic Press, New York